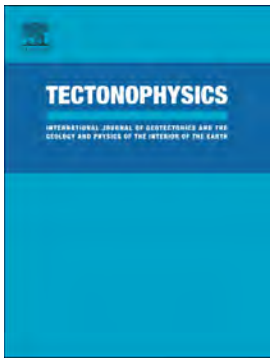

Strain variations in a seismogenic normal fault (Baza Sub-basin, Betic Chain): Insights from magnetic fabrics (AMS)

Marcos Marcén, Teresa Román-Berdiel, Antonio M. Casas-Sainz, Ruth Soto, Belén Oliva-Urcia, Julia Castro

PII: S0040-1951(19)30207-0
DOI: https://doi.org/10.1016/j.tecto.2019.05.014
Reference: TECTO 128120

To appear in: *Tectonophysics*

Received date: 9 February 2019
Revised date: 13 May 2019
Accepted date: 21 May 2019

Please cite this article as: M. Marcén, T. Román-Berdiel, A.M. Casas-Sainz, et al., Strain variations in a seismogenic normal fault (Baza Sub-basin, Betic Chain): Insights from magnetic fabrics (AMS), Tectonophysics, https://doi.org/10.1016/j.tecto.2019.05.014

Strain variations in a seismogenic normal fault (Baza Sub-basin, Betic Chain): insights from magnetic fabrics (AMS)

Marcos Marcén [a,*], Teresa Román-Berdiel [a], Antonio M. Casas-Sainz [a], Ruth Soto [b], Belén Oliva-Urcia [c], Julia Castro [d]

a Geotransfer, Dpto. Ciencias de la Tierra, Facultad de Ciencias, Instituto de Investigación en Ciencias Ambientales (IUCA), Universidad de Zaragoza, 50009 Zaragoza.

b IGME, Instituto Geológico y Minero de España, Unidad de Zaragoza, 50006 Zaragoza.

c Dpto. Geología y Geoquímica, Fac. Ciencias (6-406), Universidad Autónoma de Madrid, Ciudad Universitaria de Cantoblanco, 28049 Madrid, Spain.

d Dpto. Ciencias de la Tierra y del Medio Ambiente, Universidad de Alicante, 03690 Alicante, Spain.

* Corresponding author: mma@unizar.es

Abstract

AMS and structural analysis are here applied to study the deformed zone associated with a large-scale, active normal fault in the central Betic Cordillera (Spain), namely the Baza fault system, to determine: i) the kinematics of structures and their relation with fault zone architecture and segmentation degree, ii) the correlation between deformational structures and the different types of magnetic fabrics and iii) the evolution of magnetic fabrics patterns, from sedimentary to shear-related, associated with normal faults. Five outcrops (969 samples) were analysed along the fault trace, which shows different degrees of segmentation along strike and strong localization of deformation along narrow fault zones. A first, main set of magnetic fabric data corroborates the normal kinematics of the Baza fault, showing magnetic lineations parallel to the dip-slip, transport direction. A second, secondary set of magnetic lineations, is parallel to the intersection lineation,

and can be related to less intense deformation in the fault rocks. Furthermore, a detailed study (523 samples) of a trench excavated across the fault zone, where two fault splays tend to coalesce in a linkage relay zone indicates that i) lithology and distance to fault planes are two factors that control the development of extension-related magnetic fabrics in weakly deformed sediments, ii) the development of shear-related fabrics in fault zones entails the mechanical rotation of minerals , iii) different orientation of magnetic lineations are related to different intensity of bulk deformation and iv) magnetic lineation is useful to define local deviations of deformation axes produced by changes in the local extension direction (from fault-perpendicular to fault-parallel extension) in the linkage zone between adjacent fault splays.

Key words: Baza fault, Betic Cordillera, fault zones, magnetic fabrics, relay ramp

1. Introduction

Large normal faults usually consist of several fault segments that, in their structural evolution, link forming relay ramps or transfer zones (Larsen, 1988; Childs et al., 1995; 2016; Willemse, 1997; Gawthorpe and Leeder, 2000; Walsh et al., 2003; Soliva and Benedicto, 2004). Kinematically, these zones are characterized by stress and strain perturbations and consequently breached by minor, oblique faults. These zones accommodate and transfer the displacement between different fault segments (e.g. Peacock and Sanderson, 1991; 1994; Crider and Pollard, 1998; Gupta and Scholz, 2000; Ferrill and Morris, 2001), thus contributing to the architecture of large-scale fault zones. The analysis of fault segmentation is crucial to characterize their seismogenic behaviour, because during failure Coulomb stress is enhanced around fault tips causing rupture jumps to adjacent segments (e.g. Manighetti et al., 2009; Finzi and Langer, 2012). Consequently, the geometrical and kinematic characterization of seismogenic faults is fundamental for the understanding of earthquake mechanics and hazard related to natural and/or triggered earthquakes (Sibson, 1977; 2003; Rutter et al., 1986; Jackson and White, 1989; Machette et al., 1991; Cowie, 1998). On the other hand, deformation within fault zones under

near-surface conditions is associated with strain partitioning and with the poor development of kinematic indicators due to the chaotic brecciation of fault rocks and the absence of clear foliations and mineralogical lineations. The analysis of Anisotropy of Magnetic Susceptibility (AMS or magnetic fabrics) represents a powerful technique to identify the rock petrofabric (e.g. Graham, 1954; Hrouda, 1987, 1993; Borradaile and Tarling, 1981; Tarling and Hrouda, 1993; Borradaile and Henry, 1997; Borradaile and Jackson, 2004). This technique is especially useful in scenarios of low-strain, brittle fault zones because of its proved ability to average the orientations of the whole set of petrofabric elements and, therefore, to provide a finite strain ellipsoid of the sheared rock (Solum and van der Pluijm, 2009; Mertanen and Karell, 2012; Levi et al., 2014; Pomella, 2014; Casas et al., 2017, 2018; Marcén et al., 2018a; Vernet et al., 2018; Román-Berdiel et al., 2018). Most previous AMS studies in brittle fault zones deal with kinematic determinations in strike-slip or reverse faults, indicating the development of magnetic lineations either parallel to the transport direction or to the intersection lineation (Fig. 1; see Parés and van Der Pluijm, 2002a; Casas-Sainz et al., 2017, 2018; Vernet et al., 2018). This ambiguity in the interpretation of the magnetic lineation within fault zones (e.g Marcén et al., 2018a) demands a proper analysis to unravel the factors involved in each type of orientation. Furthermore, AMS studies applied to the kinematic determinations in brittle, normal fault zones are scarce (see Braun et al., 2015, in the transtensive Dead Sea Fault) and usually focused on determining the distance at which the influence of the fault slips affects the orientation of magnetic lineations (e.g. Levi et al., 2014).

In this work, AMS is applied to a large NNW-SSE normal fault system located in the Betic Cordillera (Southern Spain): the Baza Fault. We have sampled four outcrops and a 16 m-long trench cutting through two fault splays. The Baza fault constitutes a significant feature in the recent evolution of the Betic Cordillera due to its seismogenic activity in recent times (García-Tortosa et al., 2008, 2011; Alfaro et al., 2010; Castro et al., 2018) and its major role in controlling the subsidence and sedimentary filling of the intramontane Baza sub-basin since the Miocene (Sanz de Galdeano et al., 2007; 2012; Alfaro et al., 2008; García-Tortosa et al., 2008; Haberland

et al., 2017). Lacustrine sedimentation during Pliocene times favoured a continuous deposit of syntectonic water-laid, non-consolidated, siliciclastic sediments. These sediments ususally provide reliable strain information from magnetic fabric analyses, due to the development of preferred mineral orientation both under compressional (Sagnotti and Speranza, 1993; Aubourg et al., 1995; Mattei et al., 1995; Soto et al., 2009; Pueyo-Anchuela et al., 2010; Gómez- Paccard et al., 2012) and extensional regimes (Sagnotti et al., 1994; Mattei et al., 1997; 1999; Cifelli et al., 2005; Soto et al., 2007; 2008; 2012; Oliva-Urcia et al., 2010a,b; 2013; Pueyo-Anchuela et al., 2011; García-Lasanta et al., 2013; 2014; 2015; 2018).

The goal of our work is two-fold: i) from the methodological point of view, we try to better define the factors controlling the development of extension-related magnetic lineations (Figs. 1a, b) and the magnetic fabric related to shear processes within normal fault zones (which has remained practically unstudied until this work, Figs. 1b, c), and ii) from the regional point of view, we aim to characterize in detail the kinematics and architectural variations along the segmented Baza fault system.

2. Geological setting

The Betic Cordillera is a consequence of the NNW-SSE convergence between Africa and Europe since the Miocene, at a rate of 4-5mm/year. This convergence co-habited with ENE-WSW orogen-parallel extension (Galindo Zaldívar et al., 1999; Sanz de Galdeano and López-Garrido, 2000; Marín-Lechado et al., 2005), that resulted in the development of intramontane basins (e.g. Granada and Guadix-Baza basins) limited by NNW-SSE extensional fault systems (Galindo-Zaldívar et al., 1999; Peña, 1979, 1985; Viseras, 1991; Gibert et al., 2007; Fig. 2a). The Guadix-Baza basin, located in the central area of the Betic Cordillera, has been traditionally divided into two areas: the western, Guadix sub-basin and the eastern, Baza sub-basin. The Baza fault separates these two sub-basins (Alfaro et al., 2008; Figs. 2a, b) and controlled the structural, sedimentological and geomorphological evolution of the Baza sub-basin (Vera, 1970; 1994;

Viseras, 1991; Gibert et al., 2007). The filling of the Baza sub-basin, reaching 2200m of sediment thickness (Alfaro et al., 2008; Haberland et al., 2017), started in Miocene times with the sedimentation of marine deposits. During Pliocene/Pleistocene times the uplift of the Betic Cordillera produced a transition to continental environments (Vera, 1970a, b; Peña, 1979, 1985; Agustí, 1986; Viseras, 1991; Guerra-Merchán, 1992; Vera et al., 1994; Agustí et al., 1997; Soria et al., 1998). From this period onwards, the activity of the Baza fault imposed important differences in sedimentary environments: proximal, fluvial in the Guadix sub-basin, and endorheic fluvial and lacustrine in the Baza sub-basin, as a consequence of the higher subsidence in the hangingwall of the Baza fault (Sanz de Galdeano et al., 2007; 2012; Alfaro et al., 2008). The filling of the Baza sub-basin ended in middle Pleistocene times, when the endorheic area and its drainage were captured by the Guadalquivir fluvial network. During the Quaternary, sedimentation was restricted to depressed areas, and alluvial fans and piedmont systems developed (Fig. 2b). These deposits are frequently offset due to the recent activity of the Baza Fault, producing stepped fault scarps (García-Tortosa et al., 2008; 2011; Castro et al., 2018).

The Baza fault system shows an along-strike length of about 37 km, its strike varying from N-S in its central sector (the area studied in this work), to NW-SE in its southernmost sector. The average dip of fault segments is 45-60° E (Fig. 2b). The accumulated throw is ca. 2000-3000 m (Alfaro et al., 2008; García-Tortosa et al., 2008; 2011). Along strike, the fault shows different degrees of segmentation: in its northern sector, the Baza fault is formed by two main strands, while in the southern sector it consists of, at least, 13 fault splays (Alfaro et al., 2008). This segmentation also implies a change in the width of the faulted zone, ranging between 0.2 km to the North to more than 7 km in the South (Figs. 2b, c). The activity of the fault has been studied in several, recent works, remarking the importance of its recent activity by means of paleosismological, geomorphological and structural techniques. These works report vertical slip rates between 0.17 and 0.49 mm/year (Alfaro et al., 2008; García-Tortosa et al., 2011; Sanz de Galdeano et al., 2012) and 8-9 seismic events in the past 45,000 years (Castro et al., 2018). The Baza fault is responsible for the 1531 Baza earthquake (Ms 6.0; VIII-IX), the most important

historical earthquake recorded in southern Iberia (Alfaro et al., 2008; Sanz de Galdeano et al., 2012).

3. Methodology

A combination of structural analysis and magnetic techniques (AMS analyses and magnetic mineralogy experiments) was used to characterize the geometry and kinematics of the Baza fault system and associated fault rocks. All the samples were collected from seven outcrops located in the central sector of the Baza fault system (Fig. 2). Five outcrops are located within the fault zone (Cañada del Gallego, Cueva Gil, La Tejera, El Carrizal trench, Piedras Rodadas outcrops; see Fig. 2 and Table 1) and two outcrops in Pliocene deposits of its footwall.

In all outcrops, except for the El Carrizal trench, samples were obtained from oriented hand blocks and cut to 2.1 cm-side cubes by means of a trim saw. In el Carrizal trench (a 16 m long, 3 m deep trench showing an E-W direction, perpendicular to the fault trend) a detailed study was carried out by sampling 523 AMS specimens (Table 1). Samples were collected from the northern wall of the trench by means of a portable electric drill, and oriented in situ with an orientation device. The western wall (1.5x3 m) of the trench was also sampled in order to discard that drilling procedures had any imprint in AMS orientation.

3.1. Structural analysis

Bedding, discrete shear bands, foliation planes, SC structures and striae were measured and represented in stereoplots using the Stereonet software (Allmendinger et al., 2012). Additionally, hydroplastic faults and their striae were measured in AMS samples. We performed paleostress analysis of fault planes and striae to determine the local stress tensor by two different methods: i) Etchecopar method (Etchecopar et al., 1981; Etchecopar, 1984) using Faille software (Célerier et al., 2011) and, ii) Right Dihedra method (Pegoraro, 1972; Angelier and Mechler, 1977) using FaultKin software (Marrett and Allmendinger, 1990; Allmendinger et al., 2012).

A microstructural study was also carried out in 24 thin sections oriented perpendicular to observed foliation, bedding planes or magnetic foliation (k_{max}-k_{int} plane), and containing either the transport direction (XZ section of the finite strain ellipsoid) or the intersection lineation (YZ section). In sites without kinematic indicators, we used the magnetic lineation as a reference for cutting the thin sections.

3.2. Magnetic techniques: RT-AMS, LT-AMS and κ-t curves

The magnetic analyses consisted of low-field AMS at room (RT-AMS) and low (LT-AMS) temperature and thermomagnetic curves (*κ-t curves*). Measurement of RT-AMS was done in a total of 1077 standard specimens with a KLY-3S Kappabridge (Agico Inc., Czech Republic) in the Magnetic Fabrics Laboratory of the University of Zaragoza. The obtained data provide the orientation and magnitude of the $k_{max} \geq k_{int} \geq k_{min}$ axes of the AMS ellipsoid, defining the orientation of the magnetic lineation (k_{max} axes) and the magnetic foliation (plane perpendicular to k_{min} axes). The magnetic ellipsoid is also characterized by two scalar parameters (Jelinek, 1981): i) the corrected degree of anisotropy (P' or Pj), which provides information about magnetic minerals and their degree of preferred orientation, and ii) the shape parameter (T), varying between $0 \geq T \geq -1$ (prolate ellipsoids) and $0 \leq T \leq 1$ (oblate ellipsoids). The average directional and scalar value for each site was calculated using Jelinek's (1978) statistics with Anisoft 4.2 (Chadima and Jelinek, 2009).

LT-AMS measurements were carried out in 4 sites (23 specimens) in order to enhance the paramagnetic contribution following the Curie-Weiss law for paramagnetic behaviour: $K_{para} = C/T-\Theta$, where K_{para} is the paramagnetic susceptibility, C is the Curie constant and Θ is the paramagnetic Curie temperature (Ihmlé et al., 1989; Ritcher and Van der Plujim, 1994; Biedermann et al., 2014). Therefore, the increase in the bulk susceptibility at LT is also used as indicator of the contribution of the paramagnetic fraction to the total RT-AMS (Lüneburg et al., 1999). With this procedure, the paramagnetic sub-fabric can be isolated from the total magnetic fabric (Lüneburg et al. 1999; Parés and Van der Pluijm 2002b; Martín-Hernández and Ferré, 2007; Oliva-Urcia et al. 2010c). To prevent instrument drift caused by the cold sample, a

thermal protection around the measuring coil of the KLY-3S Kappabridge is used (Issachar et al. 2016).

Curves of temperature variation of magnetic susceptibility (κ-T) were performed from −195 °C to 700 °C in a KLY-3S Kappabridge combined with a CS-L cryogenic apparatus and a CS-3 furnace (AGICO company) in order to determine the magnetic mineralogy in 14 samples. The measurements were done in argon atmosphere to minimize mineral reactions with oxygen during heating, and data were processed with Cureval 8.0 software (Chadima and Hrouda, 2009).

4. Structural data and outcrop description

Several splays of the fault system were analysed to determine if different degrees of segmentation have implications in kinematics and deformation. Along strike, two different zones can be distinguished: i) the northern sector, where the fault system consists of minor, segmented fault arrays and ii) the central and southern sectors, where fault displacement is distributed in up to 13 splays (Fig. 2b); in this area, transfer zones or relay ramps are expected.

4.1 Northern sector of the Baza Fault

In the northernmost sector of the studied area of the Baza fault system the total displacement of the fault is concentrated in two fault strands, exposed in the Cañada del Gallego outcrop. In this exposure, a 50 m wide fault zone is limited by two N-S, east dipping major fault planes that bring the Pliocene red silts and marls in the footwall in contact with the Pleistocene carbonate silts in the hangingwall (Fig. 3a, b). In general, the fault zone is poorly exposed with the exception of the two main fault planes, where incipient brittle SC structures (Fig. 3c) are compatible with the dip-parallel slickensides observed in discrete shear planes, indicating pure normal kinematics for both fault planes (Fig. 4a). Although small drag folds are present close to the main fault planes, bedding remains horizontal or shows shallow dips towards the E in both hangingwall and footwall.

Towards the South, the total throw of the Baza fault system is distributed in several N-S, East-dipping splays. In this sense, La Tejera (Fig. 3e) and Cueva Gil (Fig. 3f) outcrops lie on

different splays of the fault system, with apparently lower fault throws than in the Cañada del Gallego outcrop. For this reason, fault zones developed in both outcrops are also narrower than in Cañada del Gallego outcrop, and strain is strongly localized in a 1 m wide zone in both outcrops, showing well-developed, brittle SC structures (Fig. 3d, f). In Cueva Gil outcrop, Pliocene red silts and marls appear in both blocks of the fault. Meanwhile, in La Tejera outcrop the Pleistocene silts are in contact with the Pliocene silts. As in the Cañada de Gallego outcrop, kinematic indicators (incipient brittle SC structures and slickensides) agree with a normal component in both splays (Fig. 4a). Although dynamic analysis for these northern outcrops were not performed because of the scarce number of fault planes observed and measured, the presence of N-S normal faults with dip-parallel striae (Fig. 4a) is consistent with the regional ENE-WSW extension direction described in previous works (Galindo Zaldívar et al., 1999; Sanz de Galdeano and López-Garrido, 2000; Marín-Lechado et al., 2005).

In thin sections from these outcrops, normal brittle SC structures are observed along the XZ sections of the strain ellipsoid, with phyllosilicate grains clearly visible and their basal planes oriented parallel to shear bands and foliation planes (Fig. 3c, d). In the Cañada del Gallego outcrop, SC structures are better developed in the eastern fault plane (Bz17 AMS site, Fig. 3a) than in the western one (Bz20, Fig. 3b). The absence of deformational structures along the YZ section of the strain ellipsoid is compatible with simple shear deformation and also with the interpretation of a normal movement for this fault. In the hangingwall of the Baza fault in the Cañada del Gallego outcrop (Bz18), basal planes of phyllosilicates are contained on bedding surfaces.

4.2 Central sector of the Baza Fault; El Carrizal trench

Unlike previously described outcrops, El Carrizal trench shows a complex, 7 m wide fault zone developed between two N-S, E-dipping strands of the Baza fault system, which tend to

coalescence at this point (Fig. 5a). The trench, perpendicular to the main fault slip surfaces, comprises the whole fault zone, the footwall and the hangingwall.

At the footwall, where white carbonate silts and brown detrital Pliocene rocks crop out, a set of synthetic and antithetic minor fault planes are arranged in horst and graben geometry with decimetric to metric throws and millimetric shear zones (Fig. 5a, b). These faults delimit extensional horses having relatively low internal deformation and bedding planes are preserved practically undisturbed within them (Fig. 5b). However, hydroplastic, striated surfaces with millimetric to centimetric throws are frequent (i.e. Fig. 5d). Within the fault zone, the most-brecciated, fault core corresponds with the main western fault plane, and a 7 m wide damage zone appears between this plane and the eastern fault plane (Fig. 5a, c). Lithologically, the fault core is a mixture of silts from the footwall and brown clays injected from the hangingwall. The role of the clay smear in the geometry and development of the Carrizal fault zone is described in Medina-Cascales et al. (2019). Within the damage zone, major synthetic and minor antithetic faults delimit small-sized horses showing stronger internal deformation, although bedding can still be recognized (Fig. 5c, g, h). The damage zone comprises alternating carbonate silts and clays.

Observations in thin sections indicate that bedding surfaces are present within horses (Fig. 5d, e, h, g) and only in fault zones (Fig. 5f) have they been apparently obliterated by the tectonic overprint. The different orientation of thin sections, (vertical N-S and E-W), allow us to complete the observations under the naked eye, which are critically conditioned by the E-W orientation of the trench wall. Several normal faults showing millimetric throw are observed both in N-S and E-W sections in samples collected from horses, suggesting that the total normal heave of the fault is distributed not only in E-W displacement, which can be even absent (Fig. 5e), but also in N-S displacements. In these samples, basal planes of phyllosilicates are parallel to bedding planes (Fig. 5e). Attending to fault zones, deformational structures are scarce and thin sections are characterized by cataclastic bands without clear kinematic indicators (Fig. 5f), especially in comparison with the northernmost outcrops where SC structures are present (Fig. 3c, d).

Minor faults and hydroplastic fractures within the fault zone and the footwall show a main NW-SE direction oblique to the mapped trace of the fault system and also to the two main splays analysed in the trench (Fig. 4b). Nevertheless, they show a higher dispersion in their strike (reaching WNW-ESE and N-S directions) and dip (synthetic or antithetic). Striae on fault surfaces and hydroplastic fractures show a best fit in a NE trend although they also show horizontal NW-SE rakes evidencing a higher complexity in the strain distribution in comparison with the previously described outcrops. These fault planes fit in orientation with the main fault sets identified in Medina-Cascales et al. (2019) in the Carrizal trench. Strikingly, bedding planes strike oblique (NW-SE) to the trace of the Baza fault (N-S), dipping shallowly towards the NE both in the footwall and the fault zone.

Taking into account the strong dispersion in fault strikes and rakes of striae observed in the trench, especially in comparison with the northern sector, paleostress analysis was performed in order to check their compatibility with the regional ENE-WSW extension direction. Hydroplastic faults show similar orientations indicating that there is no bias related to the size of the faults and thus validating structural and dynamic considerations obtained from the hydroplastic fractures. The result obtained by the Right Dihedra method shows a vertical σ1 which agrees with the extensional regime. However, the extension direction or σ3 is not accurately defined by this method, since nearly 90% (28 out of 30) of the faults are explained by a σ3 that ranges from NNE-SSW to E-W (Fig. 4c), with a maximum in N050E. Fortunately, Etchecopar's method (25 out of 30 faults explained) strongly constrains the orientation of σ3 to NNE-SSW (N024E ±014°), which, however, does not fit with the regional ENE-WSW extension direction (Fig. 4c).

4.3 Southern sector of the Baza Fault

The Southern sector of the studied area of the Baza fault system is characterized by the occurrence of several fault splays (Fig. 2b). Piedras Rodadas outcrop lies on one of these splays, keeping similarities with the Carrizal trench since kinematic indicators are not compatible with a pure dip-slip fault movement. The single fault plane strikes N160E, dipping 40° to the E and striae

on its surface show a rake of 55° N (Fig. 3g). Deformational patterns such as SC structures are absent in the sheared zone, and both in the hangingwall (Pleistocene carbonate silts) and footwall (Pliocene carbonate silts) bedding remains horizontal.

5. Magnetic mineralogy and LT-AMS

The 14 temperature-dependent magnetic susceptibility curves show hyperbolic shapes both at low temperature and at the initial stages of the heating curves, suggesting a dominance of the contribution of paramagnetic phases (phyllosilicates) to the total magnetic susceptibility (Fig. 6a, b, c). Sharp decreases of susceptibility around the Curie temperatures associated with possible ferromagnetic phases are absent. In heating curves, strong increases in the magnetic susceptibility are observed in the cooling paths in most samples, associated to neoformation of magnetite during the heating run (Fig. 6a, c).

The comparison between AMS measurements at low (around 77k) and room temperature corroborates the paramagnetic behaviour of the samples, since high k_m-LT/k_m-RT ratios were obtained in all sites, ranging between 3.06 and 3.84 (Fig. 6d) (3.8 is the value for a perfect paramagnetic component, see Lüneburg et al., 1999, Parés and van der Pluijm, 2002b; 2014). Furthermore, the orientation of LT-AMS overlaps in most sites the orientation of the RT-AMS (Fig. 6e). Only Group 9 (samples collected at 5 cm from fault planes in the Carrizal Trench) shows different orientation of k_{max} axes, changing from a northerly orientation of k_{max} axes at RT to a NW orientation of k_{max} axes at LT. Therefore, a small contribution from ferromagnetic minerals to define magnetic lineations cannot be totally discarded, even when this site shows the highest k_m-LT/k_m-RT ratio.

The importance of these results (i.e. dominance of contribution of paramagnetic phases, mainly phyllosilicates) lies on the straightful interpretation of RT-AMS magnetic ellipsoids in terms of magnetic lineation as a tectonic indicator of the extensional direction (see Cifelli et al., 2005) and as strain marker in fault zones.

6. Magnetic properties

6.1 Northern sector of the Baza Fault

The average scalar parameters per site are shown in Table 1 and per outcrop in Fig. 7. Outcrop-averaged bulk susceptibility values are 155 (standard deviation, e.: 30), 139 (e.: 32) and 172 (e.: 18)*10^{-6} SI in samples collected in fault zones at Cañada del Gallego, Cueva Gil and La Tejera, respectively, which fit within typical paramagnetic ranges (Rochette, 1987). Corrected degree of anisotropy (Pj) values are lower in the Cañada del Gallego outcrop (Pj: 1.030; e.: 0.010), than in Cueva Gil (Pj: 1.060; e.: 0.016) and La Tejera (Pj: 1.059; e.: 0.009). No correlation between Km and Pj is observed per site or outcrop (Fig. 7a). Shape parameter (T) is positive at all sites ranging between 0.105 and 0.790, indicating oblate shapes of the magnetic ellipsoid.

In the northern sector of the studied area there is a strong relationship between the observed structures and AMS data. In general, triaxial ellipsoids were obtained in all sites in the Cañada del Gallego, Cueva Gil and La Tejera outcrops (Figs. 8a, b, c). In Cañada del Gallego, samples collected within the fault zone (Bz 17, 19, 20; Fig. 8a) show their k_{min} axes perpendicular to the fault surfaces but not always well clustered (Bz 17; Fig. 8a), whereas in samples located in the hangingwall, up to 4 m far from the eastern fault plane B (Bz 18; Fig. 8a), k_{min} axes are perpendicular to the horizontal bedding plane and the k_{max} axes are strongly clustered around a horizontal NW-SE trend. Within the fault zone, k_{max} axes show different orientation in each site: i) well clustered and parallel to the dip of the fault planes and therefore parallel to the transport direction of the normal fault (Bz17), ii) the average of the k_{max} axes is parallel to the strike of the fault plane (Bz20, located in the sheared footwall, Fig. 3a, b), and iii) following a girdle distribution with k_{int} axes on the fault plane (Bz19).

In contrast to the Cañada del Gallego outcrop, Cueva Gil and La Tejera outcrops show constant, well-grouped AMS axes both within fault zones and outside the fault zones blocks. All sites collected in fault zones (Bz13, 14, 16a, b, c; Fig. 8b, c) show k_{min} axes perpendicular to the

fault planes with slight deviations, especially in the Cueva Gil outcrop (Bz16; Fig. 8b). In the footwall, k_{min} axes are perpendicular to the horizontal bedding plane (Bz15). Attending to the orientation of magnetic lineations, k_{max} axes are parallel to the dip of N-S trending fault surfaces, consistent with the observed striae/transport direction in all sites. Similarly to the Cañada de Gállego hangingwall, the results from the footwall in La Tejera outcrop show k_{max} axes contained in the bedding plane and showing a horizontal, WNW-ESE trend (Bz15; Fig. 8c). These results indicate the heterogeneous deformation of brittle fault zones and emphazise the need for analysing several sites per outcrop to obtain complete and reliable information.

6.2 Central sector of the Baza Fault; El Carrizal trench

The 523 specimens from El Carrizal trench were firstly classified by lithologies, based on their different magnetic susceptibility and scalar parameter values (Figs. 7d, e; Table 1). In the footwall of the main fault (see location in Figs. 9a, b), the dark clays and sands (Groups 1-4) have relatively high magnetic susceptibility and Pj values (Km: $55*10^{-6}$ SI; Pj: 1.022; Fig. 7d and Table 1 for standard deviations), different from the low magnetic susceptibility and Pj values (Km: $26*10^{-6}$ SI; Pj: 1.015; Fig. 7d) of white carbonate silts (Groups 5-8). These values also differ from the values of the samples collected in the western main fault trace (Km: $93*10^{-6}$ SI; Pj: 1.015; Fig. 7d), from a cataclastic mixture of carbonate silts from the footwall and dark clays from the hangingwall (Fault 1 in Fig. 9b). On the other hand, the samples from the fault zone (Fig. 9b) show a homogeneous lithology (light brown sand and clays), and specimens were grouped based on their location in the different horses (Gr 9, 10, 10b, 11, 12 and 13), which are delimited by the main fault surfaces. Bulk susceptibility values of these samples ($90*10^{-6}$ SI) are similar to the ones obtained in samples from the main fault (Fault 1) and minor fault traces (Fault 2, 3, 4, 5) but Pj values are higher (1.022; Figs. 7d, e, f). See Table 1 and for scalar parameters in faults 2, 3, 4, 5.

Groups 1 to 4 (Fig. 9a) are characterized by oblate ellipsoids with a strong clustering of k_{min} axes perpendicular to the NNE-dipping bedding planes and a girdle distribution of k_{max} and k_{int} axes within the bedding plane (typical sedimentary fabric), although a weaker clustering of k_{max} axes with a N orientation can be observed. Groups 5 to 7 and group 8 (Fig. 9a) show triaxial ellipsoids, with a weaker dispersion of k_{min} and k_{max} axes showing a clear N-S trend, close to the dip of the bedding (subhorizontal in Fig. 9a since AMS data were restored to horizontal bedding).

Samples collected from Fault 1 show k_{min} axes perpendicular to the fault plane and magnetic lineations tend to be slightly scattered, but parallel, to the strike of the N-S fault plane (Fig. 9a). Within the fault zone, the samples collected from individual fault planes (Fig. 9b) show k_{min} axes perpendicular to the fault plane, whereas k_{max} axes show different patterns: i) girdle distribution with k_{int} axes on the planes of faults 2 and 5; ii) parallel to fault strike, although slightly scattered, in the NW-SE fault 4 and iii) dip-parallel in the N-S fault 3, which is in agreement with the E-W-trending magnetic lineation observed in its footwall (Gr10b).

All the horses within the fault zone (Gr 9-13, Fig. 9b) are characterized by oblate ellipsoids with stronger clustering for k_{min} than for k_{max} axes. The k_{min} axes cluster around the poles of the bedding planes. In general, k_{max} axes are scattered, together with k_{int} axes, within the bedding planes (Gr 9, 10, 12 and 13), and only in two groups k_{max} axes are well-grouped: i) Gr10b shows magnetic lineations in a E-W trend and ii) Gr11 shows magnetic lineation with a NW-SE trend.

Taking into account that k_{max} axes show in general a girdle distribution within the horses, which is the typical situation of an undisturbed sedimentary fabric, specimens were secondly classified based on the distance from main fault planes in order to investigate its influence in the orientation of the magnetic lineation (Fig. 10). We arbitrarily chose this distance according to sampling density and lithon size. Samples from Gr1-4 (light brown clay) collected at less than 10 cm from fault planes show a better clustering (k_{max} conf. ang.: 22/10) of the magnetic lineation in a N-S direction, whereas samples collected farther from the fault show a girdle distribution of k_{max} and k_{int} axes (k_{max} conf. ang.: 69/14). The clustering of the magnetic lineation is also observed

in Gr9 or Gr13 (fault zone) among the specimens collected at less than 5 cm from minor fault planes (Fig. 10), showing a well-clustered N-S or NE-SW magnetic lineation, respectively. In Gr5-7 (white carbonate silts), where N-S magnetic lineations were previously observed, k_{max} axes remain in this direction in the samples collected closer than 10 cm to fault planes. Finally, other groups (i.e. Gr10) do not show any change in the magnetic lineation as a function of distance (Fig. 10). Looking at Km, Pj or T values of the two groups of samples collected close to or far from fault planes (Fig. 10), it is clear that scalar values show no significant change, even when there are changes in the clustering of the magnetic lineation between the two groups.

6.3 Southern sector of the Baza Fault; Piedras Rodadas outcrop

In this outcrop, bulk susceptibility values per site range between 45 and $85*10^{-6}$ SI, and Pj values show large variations, ranging between 1.007 and 1.070 (Figs. 7a, b and Table 1). AMS ellipsoids are characterized by oblate and prolate-triaxial distributions in the footwall and the fault zone-hangingwall, respectively (Fig. 8d). Within the footwall, k_{min} axes are perpendicular to bedding planes in Bz1 and Bz2 and they are contained within them in Bz5, where k_{min} axes show a horizontal N-S trend. In these sites, k_{max} axes orientation is not well defined, being scattered within the bedding planes in Bz1 and Bz2 or with a E-plunging trend in Bz5. Attending to the fault zone, prolate ellipsoids were obtained in the three collected sites (Bz3, 4, 6), with vertical disposition of k_{max} axes and girdle distribution of k_{min} and k_{int} axes, which is not consistent with the orientation of fault or bedding planes. In the hangingwall, where bedding plane remains horizontal and apparently undisturbed, k_{max} axes fit with the pole of the fault plane, and k_{min} axes show two clusters that fit either with the strike or the dip of the fault plane.

6.4 Footwall of the Baza fault system

In all sites sampled in the footwall of the Baza fault system (Fig. 8e), k_{min} axes are perpendicular to bedding planes. In four sites, k_{max} axes are clearly grouped on the bedding planes and parallel to the regional ENE-WSW extension direction (Bz10a, Bz10b and Bz11) or to a NE

direction (Bz8). The other site shows a sedimentary fabric with girdle distribution of k_{max} and k_{int} axes on the horizontal bedding plane (Bz9).

8. Discussion

8.1 Kinematics of the Baza fault from the structural and AMS study

The combination of structural and AMS studies presented in this work highlights that the kinematics and fault zone architecture of normal fault zones strongly depends on the degree of segmentation and the type of linkage between fault segments. Particularly, in the Baza fault system, our results show two different sectors; the northern sector (Cañada del Gallego, Cueva Gil and La Tejera outcrops) and the central and southern sectors (El Carrizal trench and Piedras Rodadas outcrops) each having lower and higher degree of fault segmentation, respectively (Fig. 11).

In the northern sector, where the fault system shows a low degree of segmentation, structural and AMS analyses indicate pure, normal displacement for all studied fault splays, based on the predominance of magnetic lineations parallel to the dip-plunging striae and to the transport direction inferred from normal SC structures (Figs. 3, 4a and Figs. 8a, b, c). The dip-slip, top-to-the E displacement is compatible with the ENE-WSW regional extension direction (Galindo Zaldívar et al., 1999; Sanz de Galdeano and López-Garrido, 2000; Marín-Lechado et al., 2005). Attending to fault zone architecture, the absence of oblique fault planes within fault zones and fault-parallel drag folds in footwalls and hangingwalls lead us to interpret these outcrops located in the northern sector as isolated faults lacking relay ramps o transfer zones (Fig. 11). When comparing the qualitatively higher displacement of the two fault splays exposed in the northermost Cañada del Gallego outcrop with the single fault splays observed in the Cueva Gil and Tejera outcrops, we also see a correlation with the width of the sheared zones, being 50 m and 1 m thick, respectively. The high variability of magnetic lineation orientation in the Cañada del Gallego outcrop suggests that deformation is more heterogeneously distributed within wider fault zones than in narrower ones, where strain is strongly localized and magnetic lineation is in

all cases parallel to the transport direction (i.e. the Cueva Gil and Tejera outcrops), in spite of their lower displacement.

In the central sector of the Baza fault system, in the Carrizal outcrop, structural and AMS analysis indicate that the kinematics and architecture of the deformed zone in the Carrizal outcrop (central sector) keep significant similarities with relay ramps described in previous works: i) relay ramps usually show oblique structures transferring the displacement between splays, including minor strike-slip components (e.g. Larsen, 1988; Peacock and Sanderson, 1991; 1994; Giba et al., 2012; Rotevant et al., 2009; Fossen et al., 2010; Fossen and Rotevant, 2016; Fig. 4b); ii) faults showing displacements along the dip direction of the ramp are frequent in case of breached relay ramps (see Fig. 8c, d in Ferril and Morris, 2001; see also Trudgill and Cartwright, 1994; Rotevant et al., 2007; Fig. 5d, e, h, g), and iii) bedding dip is oblique or parallel to the fault cut-offs (Ferril and Morris, 2001; Fossen and Rotevant, 2016 and references therein; Fig. 4b). All these structural patterns were recognized in the Carrizal trench through structural and microstructural observations, and therefore, the deformed zone limited by the two main fault splays (fault zone in Fig. 5a) is interpreted as a transfer zone or relay ramp (Fig. 11).

The results obtained from AMS and from paleostress analysis also point to interpret this outcrop as a relay ramp. Local stress perturbations within relay ramps are widely documented, including an increase of the Coulomb stress close to fault tips (e.g. Willemse, 1996; Crider and Pollard, 1998; Gupta and Scholz, 2002; Finzi and Langer, 2012) and a change in the extension direction from fault-perpendicular to oblique or parallel to the strike of the splays within the relay ramp (e.g. Peacock and Sanderson, 1994; Ferrill and Morris, 2001). In lithons showing clustered magnetic lineations (k_{max} axes) in the Carrizal trench, they are parallel to the strike of the fault splays, suggesting that a N-S, local extension direction could control their development. Furthermore, paleostress analysis also point to a fault-parallel local extension direction within the fault zone (NNE, approaching the perpendicular to the regional, ENE-WSW extension direction). These results indicate that: i) stress deflections within relay ramps entail changes in the strain ellipsoid with an elongation of the petrofabric elements parallel to the dip of the ramp, and ii) the

usefulness of the AMS method to identify petrofabric variations in low-strained rocks in extensional contexts, particularly in relay zones.

In the southernmost studied sector, Piedras Rodadas outcrop, the Baza fault system is segmented into several fault splays showing complex links between them. Kinematic indicators show that the displacement of the studied splay is not compatible with a pure normal, dip-slip movement as it occurs in the Carrizal trench. Bedding planes in the footwall and hangingwall remain horizontal and no oblique structures that could be interpreted as transfer structures within relay ramps have been observed. Unfortunately, AMS data are difficult to interpret since there is no clear correlation between the orientation of deformational structures and magnetic axes orientations. Therefore, this outcrop can be interpreted either as relay ramp or as isolated splay.

Our data confirm that the Baza fault system represents a strongly-segmented, large, normal fault as stated by previous works (Alfaro et al., 2008; García-Tortosa et al., 2008, 2011) validating the use of the selected methodology (combination of structural and AMS studies) to successfully analyse them. Our results also point to the high sensitivity of AMS data to detect different degrees of linkage and different fault zone architectures: fault zones related to an isolated fault *vs.* relay ramps between different fault strands (Fig. 11).

8.2 Development of magnetic fabrics in the Baza Fault: a test for the application of AMS to extensional contexts

In extensional settings, where the development of the magnetic fabric is not masked by subsequent compressional stage, it is crucial to define the transition from a sedimentary fabric to tectonic fabric, either extension- or sheared-related fabric. In simpler extensional scenarios, magnetic lineations, defined by the common axis of differently oriented basal planes of phyllosilicates, are parallel to the extension direction (Cifelli et al., 2005 and references therein). However, in complex settings, as the fault system studied here, different magnetic ellipsoid orientations can be observed in relation to the tectonic overprint. Accordingly, magnetic fabrics

evolve from sedimentary (no clustering of magnetic lineation) in low-strained extensional horses (i.e. Carrizal trench), to tectonic (clustered magnetic lineation parallel to extension direction), close to fault planes (i.e. Carrizal trench and fault blocks in the northern outcrops), and finally to magnetic lineations conditioned by shear processes within fault zones (i.e. northern outcrops). Furthermore, the Pj vs T diagram (Fig. 7b) reflect this different tectonic overprint, showing the classical evolution previously described in compressional settings (e.g. Parés and van der Pluijm., 2004; Debacker et al., 2004; 2009; Pueyo-Anchuela et al., 2012). This means a transition from sedimentary to shear-related fabrics: in Piedras Rodadas and El Carrizal trench, where sedimentary and extension-related magnetic fabrics are predominant, Pj and T values are significantly lower than in the northern outcrops, where shear-related fabrics are associated with higher Pj and T (Figs. 7b, c).

8.2.1 Development of clustered magnetic lineations in weak deformed sediments

If we consider the clustering of the magnetic lineations in extensional-related fabrics observed within the horses in the Carrizal trench (Fig. 12a), two factors seem to control their development: i) the rheology of the different lithologies and ii) the distance to fault planes. Materials containing a significant sandy fraction (Gr1-4 in the footwall and Gr9-13 in the fault zone) show fabrics whose k_{max} axes show a girdle distribution on the bedding plane, whereas white carbonate silts (Gr5-8) develop well clustered, N-S oriented k_{max} axes (Fig. 9). Considering that strain is similar within each horse and that ferromagnetic minerals are not contributing critically to the RT-AMS (k-T analysis and LT-AMS indicate paramagnetic dominance), the scattering in the magnetic lineation can be related to the presence of coarser, sandy fractions, since they can inhibit the development of the intergrain folding or kinking of phyllosilicates, which is the responsible of the development of k_{max} axes parallel to stretching direction (as shown in Cifelli et al., 2005). Medina-Cascales et al. (2019) also point the different role in strain development of clay and sandy levels in the Carrizal trench, prone to develop ductile and brittle deformation style, respectively. In addition, a direct relationship between distance to fault planes and clustering of

magnetic lineations can be inferred in the Carrizal trench. The clustering of the magnetic lineations near fault planes in several AMS groups (Fig. 10) suggests that strain localises at a distance of around ≈10 cm and that fault slip is one of the factors that controls the development of clustered magnetic lineations in non-consolidated, weakly-deformed sediments. This strain localization is probably enhanced by clay injections and smears in the surrounding areas to fault planes (Medina-Cascales et al., 2019). Furthermore, sites collected in the footwall or hangingwall in La Tejera and Cañada del Gallego are at 2 and 4 m, respectively, from the fault planes, and they also show clustered magnetic lineations, therefore influenced by nearby faults (Fig. 8a, c). In the Carrizal trench, the clustering of magnetic lineation does not imply a systematic, distinguishable change in Pj or T values (Fig. 10, 11), indicating that the intergranular folding or kinking responsible for the change in orientation change only produced a weak perturbation in petrofrabic elements inherited from sedimentation.

8.2.2 Magnetic lineations conditioned by shear processes

The results obtained in the Baza fault indicate that shear-related deformation induces the rotation of the basal plane of phyllosilicates within fault rocks (Fig. 3c, d and Fig. 5f), and consequently k_{min} axes change from perpendicular to bedding plane (depositional pattern) to perpendicular to fault planes (tectonic pattern). In the Carrizal trench, this change is translated into a noticeable decrease of Pj and T values in comparison with the ones obtained in the surrounding, extensional horses (Fig. 7e, f and Fig. 12b). This indicates that the superimposition of different anisotropy ellipsoids (linked to bedding, fault or incipient foliation planes) entails a reduction in the ordering of the petrofabric elements in the early stages of shearing (Marcén at al., 2018b). Attending to the orientation of the magnetic lineation, a strong variability is observed when deformational structures are incipient and kinematic indicators are scarce (i.e. Faults 1-5 in the Carrizal trench; Fig. 5f), making difficult their straightforward interpretation. Fortunately, the northern outcrops (i.e. Cañada del Gallego, Cueva Gil and La Tejera) show clear kinematic indicators (Fig. 3a-f; Fig. 4a) and therefore magnetic intersection lineations and parallel-transport lineations are distinguishable (Fig. 12c). In the Cañada del Gallego outcrop, a correlation exist between strain

and these different orientations: weakly deformed rocks in the footwall of fault A (Bz20 site; Fig. 3b) provide intersection lineations and lower Pj values than strongly sheared rocks in fault B (Bz17 site), where a transport-parallel magnetic lineation is observed (Fig. 12c). Between both sites (close to fault B), magnetic lineation shows a girdle distribution, intermediate Pj and higher T values (Bz19 site; Fig. 12c) that can be interpreted as an oblate ellipsoid between the two elongated end-members. Following this interpretation, we can assume that the bulk finite strain is the direct responsible for the different magnetic lineation orientations in the Baza fault. Ferromagnetic contribution defining parallel-transport magnetic lineations (Oliva-Urcia et al., 2009; Casas-Sainz et al., 2017; Román-Berdiel et al., 2018) is non-significant. Finally, Cueva Gil and La Tejera outcrops show narrow fault zones where strain is strongly concentrated and deformational structures are better developed than in Cañada del Gallego. Consistently with the hypothesis that strain controls magnetic lineations orientation in the Baza Fault, all sites show triaxial ellipsoid having k_{max} axes parallel to the transport direction and higher Pj and T values than the ones observed in the Cañada del Gallego site (Fig. 12c).

9. Conclusions

In this work, five outcrops were analysed to determine the kinematics and architecture of the Baza fault system, a seimogenic structure of the Betic Cordillera, through a combination of structural and AMS analyses. The results obtained indicate the presence of a strongly-segmented, large-scale, normal fault system whose kinematics and architecture depend on the linkage between adjacent splays. In the case of isolated faults, their kinematics is compatible with a normal displacement, based on a predominance of magnetic lineations (k_{max} axes) parallel to the top-to-the E, dip-slip transport direction. Deformational patterns (SC structures and striae) and microstructural observations, also agree with the ENE-WSW regional extension. Conversely, linking segments developed relay ramps and oblique structures. In these cases, kinematic indicators suggest transference of displacements between adjacent splays conforming the relay

zone. A local extension direction nearly parallel to the dip direction of the ramp is obtained from paleostress analysis and tracked by magnetic lineations.

From the methodological point of view, the detailed study of the Carrizal trench (523 samples), has been crucial to obtain clues about the transition from sedimentary to extension- and shear-related fabrics within normal fault zones. Lithology and distance to fault planes are the two main factors that control the development of clustered magnetic lineations in extension-related magnetic fabrics. The transition from sedimentary to shear-related fabrics is connected to the rotation of basal planes of phyllosilicates from parallel-to-bedding to parallel-to-fault-planes, a process that entails a noticeable decrease in the Pj and T values of the shear-related samples, and the coexistence of magnetic lineations parallel and perpendicular to the transport direction. The development of each type of magnetic lineation, parallel or perpendicular, is directly related to the higher or lower, respectively, amount of shear, which is strongly dependent on the localisation of shear strain in narrow fault zones, rather than on the total displacement of the fault.

Acknowledgements

Pedro Alfaro and Iván Medina are thanked for their comments and suggestions on the article. Authors are grateful to the Servicio General de Apoyo a la Investigación-SAI (Servicio de Preparación de Rocas y Materiales Duros and Servicio de Líquidos Criogénicos) of the University of Zaragoza. Financial support was granted by research project CGL2013-42670-P and BES-2014-070167 (pre-doctoral grant to M. Marcén) of the MINECO (Ministerio de Economía y Competitividad of Spain).

References

Agustí, J., 1996. Synthèse biostratigraphique du Plio-Pléistocène de Guadix-Baza (Province de Granada, Sud-Est de l'Espagne). Geobios 19, 505–510.

Agustí J., Oms O., Garcés M., Parés J.M., 1997. Calibration of the late Pliocene-early Pleistocene transition in the continental beds of the Guadix-Baza basin (southeastern Spain). Quat. Int. 40, 93–100.

Alfaro, P., Delgado, J., Galdeano, C.S., Galindo-Zaldíevar, J., García-Tortosa, F.J., López-Garrido, a. C., López-Casado, C., Marín-Lechado, C., Gil, a., Borque, M.J., 2008. The Baza Fault: A major active extensional fault in the central Betic Cordillera (south Spain). Int. J. Earth Sci. 97, 1353–1365. https://doi.org/10.1007/s00531-007-0213-z

Alfaro, P., Gibert, L., Moretti, M., García-Tortosa, F.J., Sanz de Galdeano, C., Galindo-Zaldívar, J., López-Garrido, Á.C., 2010. The significance of giant seismites in the Plio-Pleistocene Baza palaeo-lake (S Spain). Terra Nov. 22, 172–179. https://doi.org/10.1111/j.1365-3121.2010.00930.x

Allmendinger, R.W., Cardozo, N.C., Fisher, D., 2012. Structural Geology Algorithms: Vectors & Tensors. Cambridge University Press, Cambridge, England, p. 289.

Angelier, J., Mechler, P., 1977. Sur une méthode graphique de recherche des contraintes principales également utilisable en tectonique et en séismologie: la méthode des dièdres droits. Bulletin de la Société Géologique de France, 19 (7), 1309–1318.

Aubourg, C., Rochette, P., Bergmüller, F., 1995. Composite magnetic fabric in weakly deformed black shales. Phys. Earth Planet. Inter. 87, 267–278. https://doi.org/https://doi.org/10.1016/0031-9201(94)02962-B

Biedermann, A.R., Bender Koch, C., Lorenz, W.E.A., Hirt, A.M., 2014. Low-temperature magnetic anisotropy in micas and chlorite. Tectonophysics 629, 63–74. https://doi.org/10.1016/j.tecto.2014.01.015

Braun, D., Weinberger, R., Eyal, Y., Feinstein, S., Harlavan, Y., Levi, T., 2015. Distinctive diamagnetic fabrics in dolostones evolved at fault cores, the Dead Sea Transform. J. Struct. Geol. 77, 11–26. https://doi.org/https://doi.org/10.1016/j.jsg.2015.05.007

Borradaile, G.J., Tarling, D.H., 1981. The influence of deformation mechanisms on magnetic fabrics in weakly deformed rocks. Tectonophysics 77, 151–168. https://doi.org/https://doi.org/10.1016/0040-1951(81)90165-7

Borradaile, G.J., Henry, B., 1997. Tectonic applications of magnetic susceptibility and its anisotropy. Earth-Science Rev. 42, 49–93. https://doi.org/https://doi.org/10.1016/S0012-8252(96)00044-X

Borradaile, G.J., Jackson, M., 2004. Anisotropy of magnetic susceptibility (AMS): magnetic petrofabrics of deformed rocks. Geol. Soc. London, Spec. Publ. 238, 299–360. https://doi.org/10.1144/GSL.SP.2004.238.01.18

Casas-Sainz, A.M., Román-Berdiel, T., Oliva-Urcia, B., García-Lasanta, C., Villalaín, J.J., Aldega, L., Corrado, S., Caricchi, C., Invernizzi, C., Osácar, M.C., 2017. Multidisciplinary approach to constrain kinematics of fault zones at shallow depths: a case study from the Cameros–Demanda thrust (North Spain), International Journal of Earth Sciences. Springer Berlin Heidelberg. https://doi.org/10.1007/s00531-016-1349-5

Casas-Sainz, A.M., Gil-Imaz, A., Simón, J.L., Izquierdo-Llavall, E., Aldega, L., Román-Berdiel, T., Osácar, M.C., Pueyo-Anchuela, Ó., Ansón, M., García-Lasanta, C., Corrado, S., Invernizzi, C., Caricchi, C., 2018. Strain indicators and magnetic fabric in intraplate fault zones: Case study of Daroca thrust, Iberian Chain, Spain. Tectonophysics 730, 29–47. https://doi.org/https://doi.org/10.1016/j.tecto.2018.02.013

Castro, J., Martin-Rojas, I., Medina-Cascales, I., García-Tortosa, F.J., Alfaro, P., Insua-Arévalo, J.M., 2018. Active faulting in the central Betic Cordillera (Spain): Palaeoseismological constraint of the surface-rupturing history of the Baza Fault (Central Betic Cordillera, Iberian Peninsula). Tectonophysics 736, 15–30. https://doi.org/https://doi.org/10.1016/j.tecto.2018.04.010

Célérier, B., 2011. FSA: Fault and stress Analysis Software, version 33.6; http://www.bcelerier.univ-montp2.fr/

Chadima, M., Hrouda, F., 2009. Cureval 8.0: Thermomagnetic curve browser for windows. Agico, Inc.

Chadima, M., Jelinek, V., 2009. Anisoft 4.2: Anisotropy Data Browser for Windows. Agico, Inc.

Childs, C., Watterson, J., Walsh, J.J., 1995. Fault overlap zones within developing normal fault systems. J. Geol. Soc. London. 152, 535–549. https://doi.org/10.1144/gsjgs.152.3.0535

Childs, C., Manzocchi, T., Nicol, A., Walsh, J.J., Soden, A.M., Conneally, J.C., Delogkos, E., 2017. The relationship between normal drag, relay ramp aspect ratio and fault zone structure. Geol. Soc. London, Spec. Publ. 439, 355–372. https://doi.org/10.1144/SP439.16

Cifelli, F., Mattei, M., Chadima, M., Hirt, A. M., Hansen, A., 2005. The origin of tectonic lineation in extensional basins: Combined neutron texture and magnetic analyses on "undeformed" clays. Earth Planet. Sci. Lett. 235, 62–78. https://doi.org/10.1016/j.epsl.2005.02.042

Cowie, P.A., 1998. A healing–reloading feedback control on the growth rate of seismogenic faults. J. Struct. Geol. 20, 1075–1087. https://doi.org/https://doi.org/10.1016/S0191-8141(98)00034-0

Crider, J.G., Pollard, D.D., 1998. Fault linkage: three- dimensional mechanical interaction between echelon normal faults. J. Geophys. Res. Solid. 103, 24373–24391. https://doi.org/10.1029/98JB01353

Debacker, T.N., Robion, P., Sintubin, M., 2004. The anisotropy of magnetic susceptibility (AMS) in low-grade, cleaved pelitic rocks: influence of cleavage/bedding angle and type and relative orientation of magnetic carriers. Geol. Soc. London, Spec. Publ. 238, 77–107. https://doi.org/10.1144/gsl.sp.2004.238.01.08

Debacker, T.N., Hirt, A.M., Sintubin, M., Robion, P., 2009. Differences between magnetic and mineral fabrics in low-grade, cleaved siliciclastic pelites: A case study from the Anglo-Brabant Deformation Belt (Belgium). Tectonophysics 466, 32–46. https://doi.org/10.1016/j.tecto.2008.09.039

Etchecopar, A., 1984. Etude des états de contraintes en tectonique cassante et simulations de déformations plastiques (approche matématique). Unpublished Ph.D. Thesis. USTL Montpellier.

Etchecopar, A., Vasseur, G., Daignières, M., 1981. An inverse problem in microtectonics for the determination of stress tensors from fault striation analysis. J. Struct. Geol. 3, 51–65. https://doi.org/https://doi.org/10.1016/0191-8141(81)90056-0

Ferrill, D.A., Morris, A.P., 2001. Displacement gradient and deformation in normal fault systems. J. Struct. Geol. 23, 619–638. https://doi.org/https://doi.org/10.1016/S0191-8141(00)00139-5

Finzi, Y., Langer, S., 2012. Damage in step-overs may enable large cascading earthquakes. Geophys. Res. Lett. 39. https://doi.org/10.1029/2012GL052436

Fossen, H., Rotevatn, A., 2016. Fault linkage and relay structures in extensional settings-A review. Earth-Science Rev. 154, 14–28. https://doi.org/10.1016/j.earscirev.2015.11.014

Fossen, H., Schultz, R.A., Rundhovde, E., Rotevatn, A., Buckley, S.J., 2010. Fault linkage and graben stepovers in the Canyonlands (Utah) and the North Sea Viking Graben, with implications for hydrocarbon migration and accumulation. Am. Assoc. Pet. Geol. Bull. 94, 597–613. https://doi.org/10.1306/10130909088

Galindo-Zaldívar, J., González-Lodeiro, F., Jabaloy, A., 1993. Stress and palaeostress in the Betic-Rif cordilleras (Miocene to the present). Tectonophysics 227, 105–126. https://doi.org/10.1016/0040-1951(93)90090-7

Galindo-Zaldívar, J., Jabaloy, A., Serrano, I., Morales, J., González-Lodeiro, F., Torcal, F., 1999. Recent and present-day stresses in the Granada Basin (Betic Cordilleras): Example of a late Miocene-present-day extensional basin in a convergent plate boundary. Tectonics 18, 686–702. https://doi.org/10.1029/1999TC900016

García-Lasanta, C., Oliva-Urcia, B., Román-Berdiel, T., Casas, A.M., Pérez-Lorente, F., 2013. Development of magnetic fabric in sedimentary rocks: Insights from early compactional structures. Geophys. J. Int. 194, 182–199. https://doi.org/10.1093/gji/ggt098

García-Lasanta, C., Oliva-Urcia, B., Román-Berdiel, T., Casas, A.M., Hirt, A.M., 2014. Understanding the Mesozoic kinematic evolution in the Cameros basin (Iberian Range, NE Spain) from magnetic subfabrics and mesostructures. J. Struct. Geol. 66, 84–101. https://doi.org/10.1016/j.jsg.2014.05.013

García-Lasanta, C., Oliva-Urcia, B., Román-Berdiel, T., Casas, A. M., Gil-Peña, I., Sánchez-Moya, Y., Sopeña, a., Hirt, a. M., Mattei, M., 2015. Evidence for the Permo-Triassic transtensional rifting in the Iberian Range (NE Spain) according to magnetic fabrics results. Tectonophysics 651–652, 216–231. https://doi.org/10.1016/j.tecto.2015.03.023

García-Lasanta, C., Oliva-Urcia, B., Casas-Sainz, A.M., Román-Berdiel, T., Izquierdo-Llavall, E., Soto, R., Calvín, P., Moussaid, B., Ouardi, H. El, Kullberg, J.C., Villalaín, J.J., 2018. Inversion tectonics and magnetic fabrics in Mesozoic basins of the Western Tethys: A review. Tectonophysics 745, 1–23. https://doi.org/https://doi.org/10.1016/j.tecto.2018.08.005

García-Tortosa, F.J., Alfaro, P., Galindo-Zaldívar, J., Gibert, L., López-Garrido, a. C., Sanz de Galdeano, C., Ureña, M., 2008. Geomorphologic evidence of the active Baza Fault (Betic Cordillera, South Spain). Geomorphology 97, 374–391. https://doi.org/10.1016/j.geomorph.2007.08.007

García-Tortosa, F.J., Alfaro, P., Sanz de Galdeano, C., Galindo-Zaldívar, J., 2011. Glacis geometry as a geomorphic marker of recent tectonics: The Guadix-Baza basin (South Spain). Geomorphology 125, 517–529. https://doi.org/10.1016/j.geomorph.2010.10.021

Gawthorpe, R.L., Leeder, M.R., 2000. Tectono-sedimentary evolution of active extensional basins. Basin Res. 12, 195–218. https://doi.org/10.1111/j.1365-2117.2000.00121.x

Giba, M., Walsh, J.J., Nicol, A., 2012. Segmentation and growth of an obliquely reactivated normal fault. J. Struct. Geol. 39, 253–267. https://doi.org/https://doi.org/10.1016/j.jsg.2012.01.004

Gibert, L., Ortí, F., Rosell, L., 2007. Plio-Pleistocene lacustrine evaporites of the Baza Basin (Betic Chain, SE Spain). Sediment. Geol. 200, 89–116. https://doi.org/https://doi.org/10.1016/j.sedgeo.2007.03.003

Graham, J.W., 1954. Magnetic susceptibility anisotropy, an unexploited petrofabric element. Bull. Geol. Soc. Am. 65, 1257–1258.

Guerra-Merchán, A., 1992. Origen y relleno sedimentario de la cuenca neógena del corredor del Almanzora y áreas limítrofes (Cordillera Bética). Ph.D. Thesis, Univ. Granada, Spain. 237 pp

Gupta, A., Scholz, C.H., 2000. A model of normal fault interaction based on observations and theory. J. Struct. Geol. 22, 865–879. https://doi.org/10.1016/S0191-8141(00)00011-0

Haberland, C., Gibert, L., Jurado, M.J., Stiller, M., Baumann-Wilke, M., Scott, G., Mertz, D.F., 2017. Architecture and tectono-stratigraphic evolution of the intramontane Baza Basin (Bétics, SE-Spain): Constraints from seismic imaging. Tectonophysics 709, 69–84. https://doi.org/10.1016/j.tecto.2017.03.022

Hrouda, F., 1987. Mathematical model relationship between the paramagnetic anisotropy and strain in slates. Tectonophysics 142, 323–327. https://doi.org/https://doi.org/10.1016/0040-1951(87)90131-4

Hrouda, F., 1993. Theoretical models of magnetic anisotropy to strain relationship revisited. Phys. Earth Planet. Inter. 77, 237–249. https://doi.org/10.1016/0031-9201(93)90101-E

Ihmlé, P.F., Hirt, A.M., Lowrie, W., Dietrich, D., 1989. Inverse magnetic fabric in deformed limestones of the Morcles Nappe, Switzerland. Geophys. Res. Lett. 16, 1383–1386.

Issachar, R., Levi, T., Lyakhovsky, V., Marco, S., Weinberger, R., 2016. Improving the method of low-temperature anisotropy of magnetic susceptibility (LT-AMS) measurements in air. Geochemistry, Geophys. Geosystems 17, 2940–2950. https://doi.org/10.1002/2016GC006339

Jackson, J.A., White, N.J., 1989. Normal faulting in the upper continental crust: observations from regions of active extension. J. Struct. Geol. 11, 15–36. https://doi.org/10.1016/0191-8141(89)90033-3

Jelinek, V., 1978. Statistical processing of anisotropy of magnetic susceptibility measures on groups of specimens. Studia geophisica et geodetica 22, 50–62.

Jelinek, V., 1981. Characterization of the magnetic fabric of rocks. Tectonophysics, 79, 3-4, 63-67. https://doi.org/10.1016/0040-1951(81)90110-4

Larsen, P.H., 1988. Relay structures in a Lower Permian basement-involved extension system, East Greenland. J. Struct. Geol. 10, 3–8. https://doi.org/10.1016/0191-8141(88)90122-8

Levi, T., Weinberger, R., Marco, S., 2014. Magnetic fabrics induced by dynamic faulting reveal damage zone sizes in soft rocks, Dead Sea basin. Geophys. J. Int. 199, 1214–1229. https://doi.org/10.1093/gji/ggu300

Machette, M.N., Personius, S.F., Nelson, A.R., Schwartz, D.P., Lund, W.R., 1991. The Wasatch fault zone, Utah: segmentation and history of Holocene earthquakes. J. Struct. Geol. 13, 137–149. https://doi.org/https://doi.org/10.1016/0191-8141(91)90062-N

Manighetti, I., Zigone, D., Campillo, M., Cotton, F., 2009. Self-similarity of the largest-scale segmentation of the faults: Implications for earthquake behavior. Earth Planet. Sci. Lett. 288, 370–381. https://doi.org/https://doi.org/10.1016/j.epsl.2009.09.040

Marcén, M., Casas-Sainz, A.M., Román-Berdiel, T., Griera, A., Santanach, P., Pocoví, A., Gil-Imaz, A., Aldega, L., Izquierdo-Llavall, E., 2018a. Multiple movements recorded in a crustal weakness zone in NE Iberia: The Vallès-Penedès Fault revisited. J. Geodyn. 121, 96–114. https://doi.org/10.1016/j.jog.2018.07.003

Marcén, M., Casas-Sainz, A.M., Román-Berdiel, T., Oliva-Urcia, B., Soto, R., Aldega, L., 2018b. Kinematics and strain distribution in an orogen-scale shear zone: Insights from structural analyses and magnetic fabrics in the Gavarnie thrust, Pyrenees. J. Struct. Geol. 117, 105–123. https://doi.org/10.1016/j.jsg.2018.09.008

Marín-Lechado, C., Galindo-Zaldívar, J., Rodríguez-Fernández, L.R., Serrano, I., Pedrera, A., 2005. Active faults, seismicity and stresses in an internal boundary of a tectonic arc (Campo de Dalías and Níjar, southeastern Betic Cordilleras, Spain). Tectonophysics 396, 81–96. https://doi.org/https://doi.org/10.1016/j.tecto.2004.11.001

Marrett, R., Allmendinger, R.W., 1990. Kinematic analysis of fault-slip data. J. Struct. Geol. 12, 973–986. https://doi.org/https://doi.org/10.1016/0191-8141(90)90093-E

Martín-Hernández, F., Ferré, E.C., 2007. Separation of paramagnetic and ferrimagnetic anisotropies: A review. J. Geophys. Res. Solid Earth 112. https://doi.org/10.1029/2006JB004340

Mattei, M., Funiciello, R., Kissel, C., 1995. Paleomagnetic and structural evidence for Neogene block rotations in the Central Apennines, Italy. J. Geophys. Res. Solid Earth 100, 17863–17883. https://doi.org/10.1029/95JB00864

Mattei, M., Sagnotti, L., Faccenna, C., Funiciello, R., 1997. Magnetic fabric of weakly deformed clay-rich sediments in the Italian peninsula: Relationship with compressional and extensional tectonics. Tectonophysics 271, 107–122. https://doi.org/10.1016/S0040-1951(96)00244-2

Mattei, M., Speranza, F., Argentieri, A., Rossetti, F., Sagnotti, L., Funiciello, R., 1999. Extensional tectonics in the Amantea basin (Calabria, Italy): A comparison between structural and magnetic anisotropy data. Tectonophysics 307, 33–49. https://doi.org/10.1016/S0040-1951(99)00117-1

Medina-Cascales, I., Koch, L., Cardozo, N., Martin-Rojas, I., Alfaro, P., García-Tortosa, F.J., 2019. 3D geometry and architecture of a normal fault zone in poorly lithified sediments: A

trench study on a strand of the Baza Fault, central Betic Cordillera, south Spain. J. Struct. Geol. 121, 25–45. https://doi.org/10.1016/j.jsg.2019.02.003

Mertanen, S., & Karell, F., Palaeomagnetic and AMS studies on Satulinmaki and Koijarvi fault and shear zones. *Geological Survey of Finland Special Paper*, *52*, 195-226.

Oliva-Urcia, B., Larrasoaña, J.C., Pueyo, E.L., Gil, A., Mata, P., Parés, J.M., Schleicher, a. M., Pueyo, O., 2009. Disentangling magnetic subfabrics and their link to deformation processes in cleaved sedimentary rocks from the Internal Sierras (west central Pyrenees, Spain). J. Struct. Geol. 31, 163–176. https://doi.org/10.1016/j.jsg.2008.11.002

Oliva-Urcia, B., Román-Berdiel, T., Casas, A.M., Pueyo, E.L., Osácar, C., 2010a. Tertiary compressional overprint on Aptian-Albian extensional magnetic fabrics, North-Pyrenean Zone. J. Struct. Geol. 32, 362–376. https://doi.org/10.1016/j.jsg.2010.01.009

Oliva-Urcia, B., Casas, A.M., Soto, R., Villalaín, J.J., Kodama, K., 2010b. A transtensional basin model for the Organyà basin (central southern Pyrenees) based on magnetic fabric and brittle structures. Geophys. J. Int. 184, 111–130. https://doi.org/10.1111/j.1365-246X.2010.04865.x

Oliva-Urcia, B., Rahl, J.M., Schleicher, A.M., Parés, J.M., 2010c. Correlation between the anisotropy of the magnetic susceptibility, strain and X-ray Texture Goniometry in phyllites from Crete, Greece. Tectonophysics 486, 120–131. https://doi.org/10.1016/j.tecto.2010.02.013

Oliva-Urcia, B., Román-Berdiel, T., Casas, A.M., Bógalo, M.F., Osácar, M.C., García-Lasanta, C., 2013. Transition from extensional to compressional magnetic fabrics in the Cretaceous Cabuérniga basin (North Spain). J. Struct. Geol. 46, 220–234. https://doi.org/10.1016/j.jsg.2012.09.001

Parés, J.M., van der Pluijm, B. a., 2002a. Evaluating magnetic lineations (AMS) in deformed rocks. Tectonophysics 350, 283–298. https://doi.org/10.1016/S0040-1951(02)00119-1

Parés, J.M., van der Pluijm, B.A., 2002b. Phyllosilicate fabric characterization by Low-Temperature Anisotropy of Magnetic Susceptibility (LT-AMS). Geophys. Res. Lett. 29, 68-1-68–4. https://doi.org/10.1029/2002GL015459

Parés, J.M., van der Pluijm, B. A., 2004. Correlating magnetic fabrics with finite strain: Comparing results from mudrocks in the Variscan and Appalachian Orogens. Geol. Acta 2, 213–220.

Parés, J.M., van der Pluijm, B.A., 2014. Low-temperature AMS and the quantification of subfabrics in deformed rocks. Tectonophysics 629, 55–62. https://doi.org/10.1016/j.tecto.2014.03.005

Peacock, D.C.P., Sanderson, D.J., 1991. Displacements, segment linkage and relay ramps in normal fault zones. J. Struct. Geol. 13, 721–733. https://doi.org/https://doi.org/10.1016/0191-8141(91)90033-F

Peacock, D.C.P., Sanderson, D.J., 1994. Geometry and development of relay ramps in normal fault systems. Am. Assoc. Pet. Geol. Bull. 78, 147–165. https://doi.org/10.1306/BDFF9046-1718-11D7-8645000102C1865D

Pegoraro, O., 1972. Application de la microtectonique á un étude de neotectonique. Le golfe Maliaque (Grèce centrale). Unpublished Ph.D. Thesis, USTL Montpellier.

Peña, J.A., (1979). La Depresión de Guadix-Baza: Estratigrafía del Plioceno-Pleistoceno. Ph.D. Thesis, Universidad de Granada, Spain

Peña, J.A., (1985). La depresión de Guadix-Baza. Estudios Geológicos, 41:33–46

Pueyo-Anchuela, Ó., Pocoví, J.A., Gil-Imaz, A., 2010. Tectonic imprint in magnetic fabrics in foreland basins: A case study from the Ebro Basin, N Spain. Tectonophysics 492, 150–163. https://doi.org/https://doi.org/10.1016/j.tecto.2010.06.016

Pueyo Anchuela, Ó., Gil-Imaz, A., Pocoví, J.A., Lloréns, J.F.I., 2011. Acquisition and blocking of magnetic fabrics in synsedimentary structures, Eocene Pyrenees, Spain. Geophys. J. Int. 186, 1015–1028. https://doi.org/10.1111/j.1365-246X.2011.05136.x

Pueyo Anchuela, Ó., Gil-Imaz, A., Pocoví J.A., 2012. Factors affecting the record of strain fabrics at the anisotropy of magnetic susceptibility: West-Central South-Pyrenean cleavage domain (Southern Pyrenees; NE Spain). Tectonophysics 554–557, 1–17. https://doi.org/10.1016/j.tecto.2012.05.028

Richter, C., van der Pluijm, B.A., 1994. Separation of paramagnetic and ferrimagnetic susceptibilities using low temperature magnetic susceptibilities and comparison with high field methods 82, 113–123.

Rochette, P., 1987. Magnetic susceptibility of the rock matrix related to magnetic fabric studies. J. Struct. Geol. https://doi.org/10.1016/0191-8141(87)90009-5

Román-Berdiel, T., Casas-Sainz, A.M., Oliva-Urcia, B., Calvín, P., Villalaín, J.J., 2018. On the influence of magnetic mineralogy in the tectonic interpretation of Anisotropy of Magnetic Susceptibility in cataclastic fault zones. Geophys. J. Int. 216, 1043–1061. https://doi.org/10.1093/gji/ggy481

Rotevatn, A., Fossen, H., Hesthammer, J., Aas, T.E., Howell, J.A., 2007. Are relay ramps conduits for fluid flow? Structural analysis of a relay ramp in Arches National Park, Utah. Geol. Soc. London, Spec. Publ. 270, 55–71. https://doi.org/10.1144/GSL.SP.2007.270.01.04

Rotevatn, A., Tveranger, J., Howell, J.A., Fossen, H., 2009. Dynamic investigation of the effect of a relay ramp on simulated fluid flow: geocellular modelling of the Delicate Arch Ramp, Utah. Pet. Geosci. 15, 45–58. https://doi.org/10.1144/1354-079309-779

Sagnotti, L., Speranza, F., 1993. Magnetic fabric analysis of the Plio-Pleistocene clayey units of the Sant'Arcangelo basin, southern Italy. Phys. Earth Planet. Inter. 77, 165–176. https://doi.org/10.1016/0031-9201(93)90096-R

Sagnotti, L., Faccenna, C., Funiciello, R., Mattei, M., 1994. Magnetic fabric and structural setting of Plio-Pleistocene clayey units in an extensional regime: the Tyrrhenian margin of central Italy. J. Struct. Geol. 16, 1243–1257. https://doi.org/10.1016/0191-8141(94)90067-1

Sanz de Galdeano, C., López-Garrido, A.C., 1999. Nature and impact of the Neotectonic deformation in the western Sierra Nevada (Spain). Geomorphology 30, 259–272. https://doi.org/https://doi.org/10.1016/S0169-555X(99)00034-3

Sanz de Galdeano, C., Delgado, J., Galindo-Zaldívar, Marín, C., Alfaro, P., García Tortosa, F.J., 2008. Principales rasgos geológicos deducidos a partir de los mapas gravimétricos de la cuenca de Guadix-Baza. In: Sanz de Galdeano, C., Peláez, J.A. (Eds.), La cuenca de Guadix-Baza. Estructura, tectónica activa, sismicidad, geomorfología y dataciones existentes, pp. 101–110 (Granada).

Sanz de Galdeano, C., García-Tortosa, F.J., Peláez, J. a., Alfaro, P., Azañón, J.M., Galindo-Zaldívar, J., López Casado, C., López Garrido, a. C., Rodríguez-Fernández, J., Ruano, P., 2012. Main active faults in the Granada and Guadix-Baza Basins (Betic Cordillera). J. Iber. Geol. 38, 209–223. https://doi.org/10.5209/rev_JIGE.2012.v38.n1.39215.

Sibson, R.H., 1977. Fault rocks and fault mechanisms. J. Geol. Soc. London. 133, 191–213. https://doi.org/10.1144/gsjgs.133.3.0191

Sibson, R.H., 2003. Thickness of the seismic slip zone. Bull. Seismol. Soc. Am. 93, 1169–1178. https://doi.org/10.1785/0120020061

Soliva, R., Benedicto, A., 2004. A linkage criterion for segmented normal faults. J. Struct. Geol. 26, 2251–2267. https://doi.org/10.1016/j.jsg.2004.06.008

Solum, J.G., van der Pluijm, B. A., 2009. Quantification of fabrics in clay gouge from the Carboneras fault, Spain and implications for fault behavior. Tectonophysics 475, 554–562. https://doi.org/10.1016/j.tecto.2009.07.006

Soria, J.M., Viseras, C., Fernández, J., 1998. Late Miocene–Pleistocene tectono-sedimentary evolution and subsidence history of the central Betic Cordillera (Spain): a case study in the Guadix intramontane basin. Geol. Mag. 135, 565–574.

Soto, R., Casas-Sainz, A.M., Villalaín, J.J., Oliva-Urcia, B., 2007. Mesozoic extension in the Basque-Cantabrian basin (N Spain): Contributions from AMS and brittle mesostructures. Tectonophysics 445, 373–394. https://doi.org/10.1016/j.tecto.2007.09.007

Soto, R., Casas-Sainz, A.M., Villalaín, J.J., Gil-Imaz, A., Fernández-González, G., Del Río, P., Calvo, M., Mochales, T., 2008. Characterizing the Mesozoic extension direction in the northern Iberian plate margin by anisotropy of magnetic susceptibility (AMS). J. Geol. Soc. London. 165, 1007–1018. https://doi.org/10.1144/0016-76492007-163

Soto, R., Larrasoaña, J.C., Arlegui, L.E., Beamud, E., Oliva-Urcia, B., Simón, J.L., 2009. Reliability of magnetic fabric of weakly deformed mudrocks as a palaeostress indicator in compressive settings. J. Struct. Geol. 31, 512–522. https://doi.org/10.1016/j.jsg.2009.03.006

Soto, R., Kullberg, J.C., Oliva-Urcia, B., Casas-Sainz, A.M., Villalaín, J.J., 2012. Switch of Mesozoic extensional tectonic style in the Lusitanian basin (Portugal): Insights from magnetic fabrics. Tectonophysics 536–537, 122–135. https://doi.org/10.1016/j.tecto.2012.03.010

Tarling, D.H., Hrouda, F., 1993. The Magnetic Anisotropy of Rocks. Chapman and Hall, 212 pp.

Trudgill, B., Cartwright, J., 1994. Relay-ramp forms and normal-fault linkages, Canyonlands National Park, Utah. Geol. Soc. Am. Bull. 106, 1143–1157.

Vera, J.A., 1970. Estudio estratigráfico de la depresión de Guadix-Baza. Bol. Geol. Min. 91, 429-462.

Vera, J.A., Rodríguez J., Guerra-Merchán A., Viseras C., 1994. La Cuenca de Guadix-Baza. Documents et Travaux de l'IGAL, 14:1–17

Vernet, E., Casas-Sainz, A.M., Román-Berdiel, T., Marcén, M., Osácar, M.C., 2019. Variable magnetic fabrics under heterogeneous deformation across a shallow fault zone in the Iberian Chain (Monroyo thrust, N Spain) 45, 111-127. https://doi.org/10.1007/s41513-018-0090-2

Viseras, C., (1991) Estratigrafía y sedimentología del relleno aluvial de la cuenca de Guadix (Cordilleras Béticas). Ph.D. Thesis, Universidad de Granada, Spain, pp 1–344

Walsh, J.J., Bailey, W.R., Childs, C., Nicol, A., Bonson, C.G., 2003. Formation of segmented normal faults: A 3-D perspective. J. Struct. Geol. 25, 1251–1262. https://doi.org/10.1016/S0191-8141(02)00161-X

Willemse, E.J.M., 1997. Segmented normal faults: correspondence between three-dimensional mechanical models and field data. J. Geophys. Res. 1902, 675–692.

Table captions

Table 1. Summary of magnetic scalar and directional data and structural patterns.

n, number of samples; Km, average value of magnetic susceptibility (E-6 SI); Pj, corrected degree of anisotropy; T, shape parameter; e, standard deviation; kmax, kmin, mean orientations (D/I, declination/inclination); conf. angl., confidence angles; Pole S0 /F, pole to bedding or to fault in sites collected in hanging and footwall or within fault zone respectively (T/P, trend/plunge); In grey colour, sites collected in hanging or footwall, separated from sites collected within fault zones, in without colouring.

Figure captions

Fig. 1. Sketch showing the relation between deformation and magnetic fabrics. a) Sedimentary fabrics, showing magnetic foliation parallel to bedding surfaces and girdle distribution of magnetic lineations. b) Extension-related fabrics, with clustered magnetic lineations parallel to the local extension direction. c) Shear-related fabrics, with magnetic foliations parallel to fault or foliation planes and magnetic lineations parallel or perpendicular to the transport direction.

Fig. 2. a) Geological sketch of the studied sector of the Betic Cordillera. BB: Baza sub-basin; GB: Guadix sub-basin. b) Geological map of the Baza Fault, showing the location of the studied outcrops. c) Geological cross section of the Carrizal trench. Modified from Castro et al. (2018).

Fig. 3. Photographs showing four of the studied outcrops of the Baza fault system and the locations of the AMS sites. a) Cañada del Gallego outcrop; overall view of the fault zone, where the total displacement is concentrated in the single fault zone shown. B) Location of the Bz20 AMS site at the footwall in the Cañada del Gallego outcrop, just in contact with the western main fault plane (Fault A in Fig. 3a). c, d) Photomicrographs of thin sections representative of the fault rocks collected from Cañada del Gallego (c) and Cueva Gil (d) outcrops. Thin-section photographs were taken from XZ section with crossed (c) and parallel (d) polarizers, ×2.5 lens. e) La Tejera outcrop, with the studied fault splay and a detailed photograph of the observed SC structures. f) Fault zone in the Cueva Gil outcrop and SC structures developed within the narrow deformed zone. g) Piedras Rodadas exposure, with a photograph of the striated fault plane.

Fig. 4. Stereoplots showing structural data. Lower hemisphere, equal-area projections. a) Orientation of fault planes and their striae of the three northernmost studied outcrops. b) Orientation of bedding planes, fault planes and their striae measured on the Carrizal trench. c) Results of the paleostress analysis performed in the Carrizal trench. Numbers indicate the number of faults compatible with a specific σ3 orientation, determined by the Right Diehdra method; Kamb contours, contour interval 2%. Results of the Etchecopar method is shown by red (σ3) and blue (σ1) stars.

Fig. 5. a) Interpreted panorama of the Carrizal trench. The two main fault planes, the footwall, the core fault zone and the hangingwall are indicated. b) Detailed image of the lithology and structure observed in the footwall. Bedding planes remain practically undisturbed. c) Detailed image of the materials and structure observed in the fault zone, where bedding planes are stretched. d, e) Photographs of thin sections in two different orientations (shown on the photos) in samples collected from AMS Group 2 in the footwall. The absence of displacements in vertical, E-W orientations is noticeable. f) Photograph of the deformational patterns observed in Fault 1. Notice the absence of clear kinematic indicators both in the core and damage zones. g, h) Photographs of thin sections along two different orientations (shown on the photos) in samples collected from AMS Group 9 in the fault zone. Both thin sections show displacements.

Fig. 6. a, b, c) Temperature-dependent magnetic susceptibility (K–T) curves in three different outcrops. Paramagnetic behaviour dominates in all curves. d) Ratio between the magnetic susceptibility at low and room temperature (LT/RT). E) Comparison of results from the different methods used for subfabric separation: RT-AMS (orange symbols) and LT-AMS (black symbols). Lower hemisphere, equal-area projections.

Fig. 7. Diagrams showing the bulk magnetic susceptibility vs. corrected degree of anisotropy (a, d) and the corrected degree of anisotropy vs. shape parameter (b, e) by samples for all sites (a, b) and for the Carrizal trench, separated by lithology and structural criteria (d, e). In c) and f), histograms with the corrected degree of anisotropy vs. % of samples are shown. In b) and c), lines with arrow indicates the evolution of the parameters in function of increasing strain.

Fig. 8. Equal-area, lower-hemisphere projections of the magnetic ellipsoids for all sites, with the exception of the Carrizal Trench.

Fig. 9. a) Detailed image of the Carrizal trench footwall and the AMS data obtained, with the main structures and the location of the collected AMS samples and groups. B) AMS data and groups and main structural features for the core of the fault zone of the Carrizal trench. Samples

collected in fault zones are indicated by yellow dots, and samples collected within extensional horses are red dots. Lower hemisphere, equal-area projections.

Fig. 10. Second classification of the samples collected in the Carrizal trench as a function of the distance to fault planes. Histograms show the corrected degree of anisotropy vs. % of samples and diagrams show the corrected degree of anisotropy vs. shape parameter as a function of the distance to fault planes.

Fig. 11. Sketch of the Baza fault system, evidencing the different degree of segmentation of the structure, the AMS results and their interpretation. Double-arrows indicate the local extension direction (black) and the orientation of magnetic lineation (blue). Not to scale.

Fig. 12. Evolutionary model from sedimentary to shear-related magnetic fabrics in the Baza fault. a) Transition from sedimentary to extension-related fabrics controlled by lithology and structural criteria. b) Transition to shear-related fabric entails strong variability of the magnetic lineation orientation and a noticeable reduction on the Pj and T values. c) Progressive development of shear-related fabrics defines constant, magnetic lineation parallel to transport direction instead of the combination of parallel and perpendicular magnetic lineations, accompanied by an increase of Pj and T values.

Table 1. Summary of magnetic scalar and directional data and structural patterns.

Site	n	Km	e	Pj	e	T	e	k_{max} (D/I)	conf. angl.	k_{min} (D/I)	conf. angl.	Pole S_0 /F (T/P)	Striae (T/P)
Cañada del Gallego outcrop (N:37,589851°, W: 2,785631°)													
Bz20	11	106	22	1.013	0.004	0.303	0.310	179/13	46/17	285/48	20/15	252/55	085/35
Bz19	23	144	28	1.031	0.006	0.770	0.089	069/73	86/08	266/17	12/06	286/25	085/64
Bz18	35	31	3	1.028	0.004	0.052	0.004	302/03	04/04	143/87	06/04	000/90	-
Bz17	48	172	12	1.035	0.007	0.105	0.237	058/27	08/07	219/62	28/07	265/44	085/45
Cueva Gil outcrop (N: 37.541857°, W: 2.794474°)													
Bz16a	35	123	29	1.052	0.010	0.587	0.132	086/30	10/05	293/57	10/05	259/21	063/68
Bz16b	28	160	19	1.077	0.015	0.119	0.286	085/32	13/07	316/44	15/08	259/21	063/68
Bz16c	28	139	32	1.052	0.005	0.790	0.101	084/43	14/06	310/36	08/06	259/21	063/68
La Tejera outcrop (N:37,537411°, W: 2,795047°)													
Bz15	36	164	28	1.061	0.012	0.149	0.430	102/05	10/08	265/85	13/10	000/90	-
Bz14	34	173	13	1.061	0.008	0.743	0.106	032/86	22/12	268/01	12/07	277/12	077/75
Bz13	17	171	26	1.056	0.008	0.465	0.207	119/24	11/06	274/64	15/08	292/46	105/41
Piedras rodadas outcrop (N:37,478791°, W: 2,783454°)													
Bz7	48	57	10	1.070	0.032	0.210	0.350	223/59	06/03	316/02	47/03	000/90	-
Bz6	31	45	4	1.007	0.002	0.076	0.312	048/71	09/07	157/06	30/07	250/50	030/32
Bz5	24	85	14	1.010	0.003	0.215	0.363	089/47	33/07	353/06	15/06	355/74	-
Bz4	25	46	11	1.004	0.002	0.076	0.425	260/70	24/12	144/05	34/12	250/50	030/32
Bz3	8	82	13	1.038	0.010	0.192	0.459	083/80	35/04	350/01	20/04	250/50	030/32
Bz2	7	66	3	1.011	0.003	0.204	0.317	076/10	62/20	183/60	29/20	355/74	-
Bz1	8	61	4	1.009	0.003	0.377	0.487	034/20	27/09	201/69	10/08	355/74	-
Baza fault system - Footwall (N:37,507389°, W: 2,794500° and N:37,503347°, W: 2,787977°)													
Bz11	32	797	117	1.023	0.007	0.454	0.210	248/12	28/08	119/72	12/08	113/80	-
Bz10-1	23	853	106	1.035	0.017	0.049	0.494	251/17	13/05	146/40	12/05	144/80	-
Bz10-2	21	926	109	1.041	0.524	0.011	0.297	266/17	16/05	113/72	09/05	144/80	-
Bz9	16	232	32	1.011	0.003	0.531	0.219	022/00	59/07	115/82	14/06	000/90	-
Bz8	16	429	177	1.007	0.003	0.409	0.326	051/04	46/07	176/83	09/07	000/90	-
El Carrizal trench (N:37,520184°, W: 2,792893°)													
Gr1-4	96	55	26	1.022	0.007	0.689	0.194	349/04	48/13	165/86	15/12	182/61	-
Gr5-7	95	26	17	1.016	0.007	0.264	0.344	009/05	28/14	189/85	31/14	206/77	-
Gr8	17	39	8	1.018	0.490	0.257	0.257	002/20	25/12	185/71	20/07	250/57	-
Gr9	59	86	19	1.022	0.008	0.759	0.156	103/05	51/09	236/84	13/08	214/77	-
Gr10a	51	88	17	1.027	0.014	0.757	0.234	157/03	72/10	274/84	18/10	190/74	-

Gr10b	14	105	9	1.020	0.007	0.715	0.158	090/09	32/13	211/74	14/05	180/77	-
Gr11	10	115	23	1.024	0.004	0.831	0.151	128/17	28/09	261/66	16/09	200/60	-
Gr12	13	119	19	1.016	0.008	0.513	0.490	194/03	36/09	305/83	10/09	196/62	-
Gr13	33	72	27	1.017	0.006	0.674	0.227	234/04	63/12	354/83	13/10	202/66	-
Fault 1	33	93	27	1.014	0.008	0.660	0.265	335/21	36/13	221/46	17/12	234/50	-
Fault 2	43	92	28	1.013	0.005	0.653	0.230	100/15	70/16	218/59	21/14	223/56	-
Fault 3	22	95	23	1.011	0.003	0.631	0.188	130/04	36/14	228/60	21/14	254/47	077/42
Fault 4	24	90	21	1.018	0.007	0.616	0.291	083/32	35/12	257/58	12/08	273/40	-
Fault 5	13	100	20	1.015	0.006	0.691	0.215	350/30	82/11	228/42	13/10	-	-

n, number of samples; Km, average value of magnetic susceptibility (E^{-6} SI); Pj, corrected degree of anisotropy; T, shape parameter; e, standard deviation; k_{max}, k_{min}, mean orientations (D/I, declination/inclination); conf. angl., confidence angles; Pole S_0 /F, pole to bedding or to fault in sites collected in hanging and footwall or within fault zone respectively (T/P, trend/plunge); In grey colour, sites collected in hanging or footwall, separated from sites collected within fault zones, in without colouring.

Highlights

- First AMS study applied to large-scale, pure normal fault zones in brittle deformation contexts.
- Characterization of different fault zone architectures along the fault system.
- Changes and evolution of AMS ellipsoid related to different tectonic overprint.
- Stress and strain perturbation within relay ramps revealed by AMS data.
- Contribution to define the overall kinematics of the seismogenic Baza Fault System.

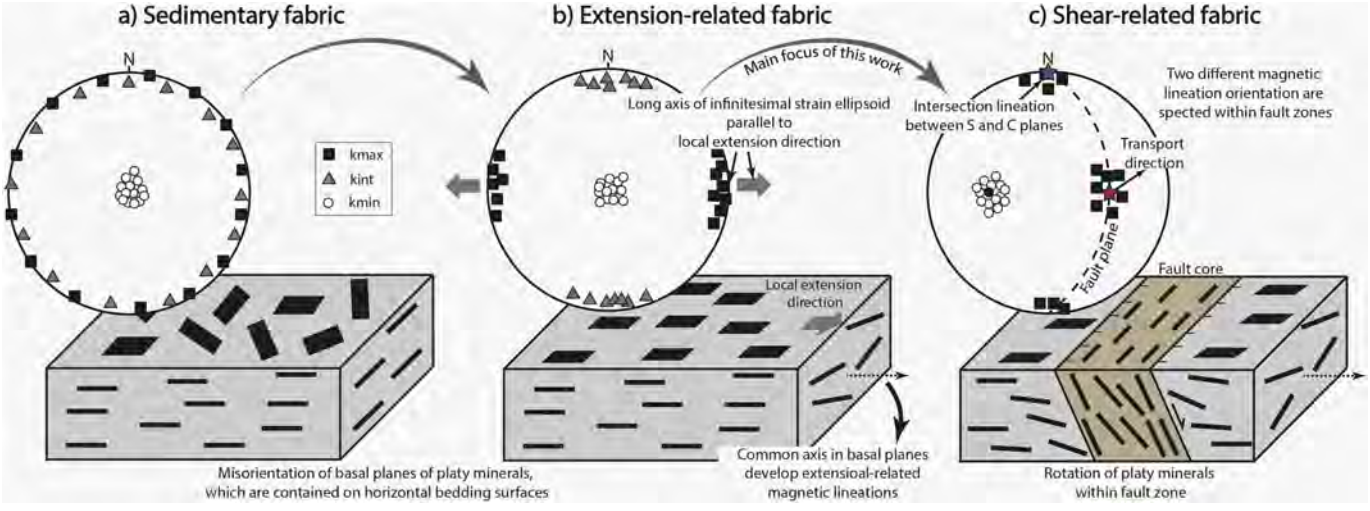
a) Sedimentary fabric
b) Extension-related fabric
c) Shear-related fabric
N
kmax
kint
kmin
Main focus of this work
Long axis of infinitesimal strain ellipsoid parallel to local extension direction
Intersection lineation between S and C planes
Two different magnetic lineation orientation are spected within fault zones
Transport direction
Fault plane
Fault core
Local extension direction
Misorientation of basal planes of platy minerals, which are contained on horizontal bedding surfaces
Common axis in basal planes develop extensioal-related magnetic lineations
Rotation of platy minerals within fault zone

Figure 1

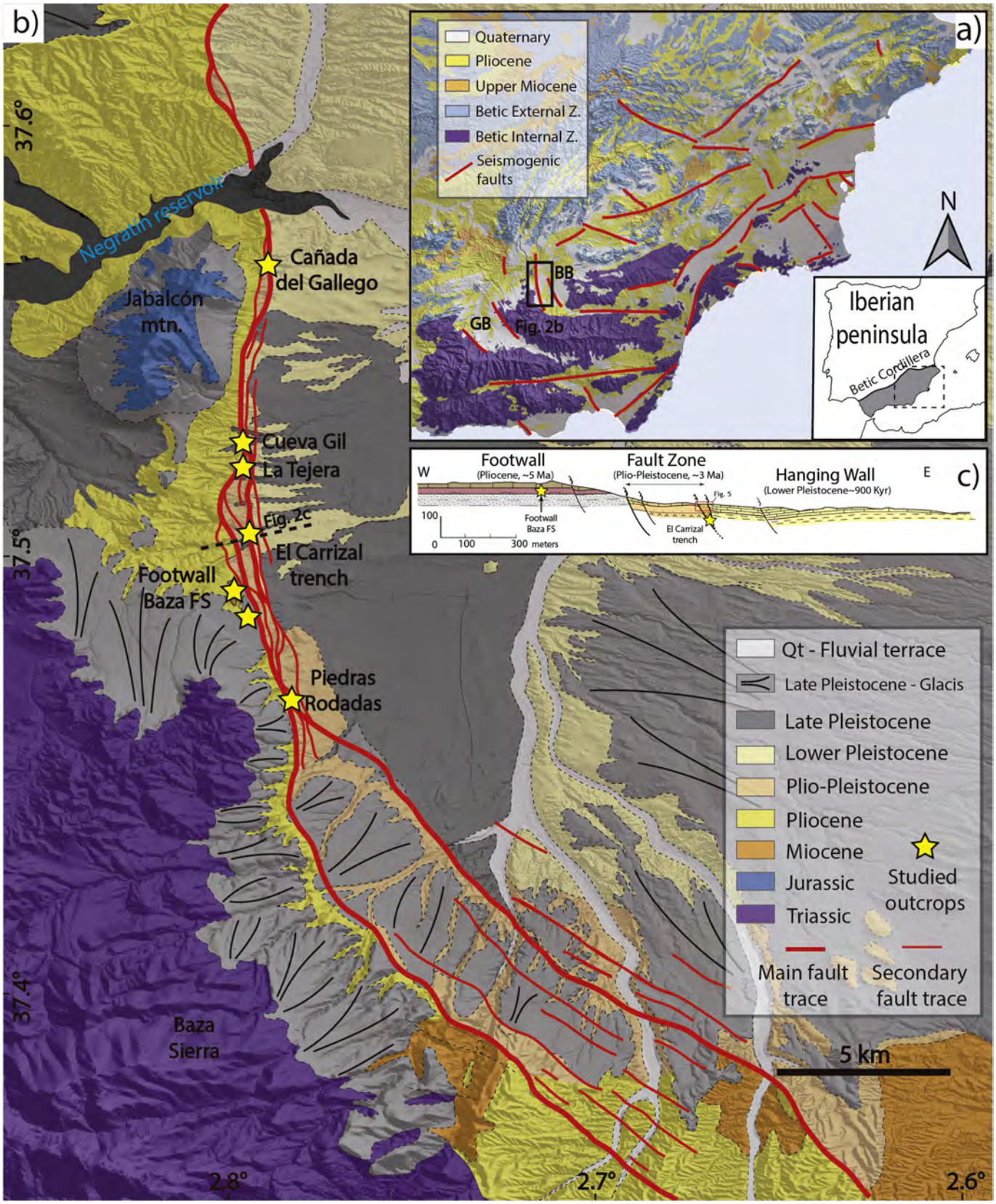
b)
a)
c)
Quaternary
Pliocene
Upper Miocene
Betic External Z.
Betic Internal Z.
Seismogenic faults
N
BB
GB
Fig. 2b
Iberian peninsula
Betic Cordillera
Negratín reservoir
Cañada del Gallego
Jabalcón mtn.
Cueva Gil
La Tejera
Fig. 2c
El Carrizal trench
Footwall Baza FS
Piedras Rodadas
Baza Sierra
W
Footwall
(Pliocene, ~5 Ma)
Fault Zone
(Plio-Pleistocene, ~3 Ma)
Hanging Wall
(Lower Pleistocene~900 Kyr)
E
Fig. 5
Footwall Baza FS
El Carrizal trench
100
0
100
300 meters
Qt - Fluvial terrace
Late Pleistocene - Glacis
Late Pleistocene
Lower Pleistocene
Plio-Pleistocene
Pliocene
Miocene
Jurassic
Triassic
Studied outcrops
Main fault trace
Secondary fault trace
5 km
37.6°
37.5°
37.4°
2.8°
2.7°
2.6°

Figure 2

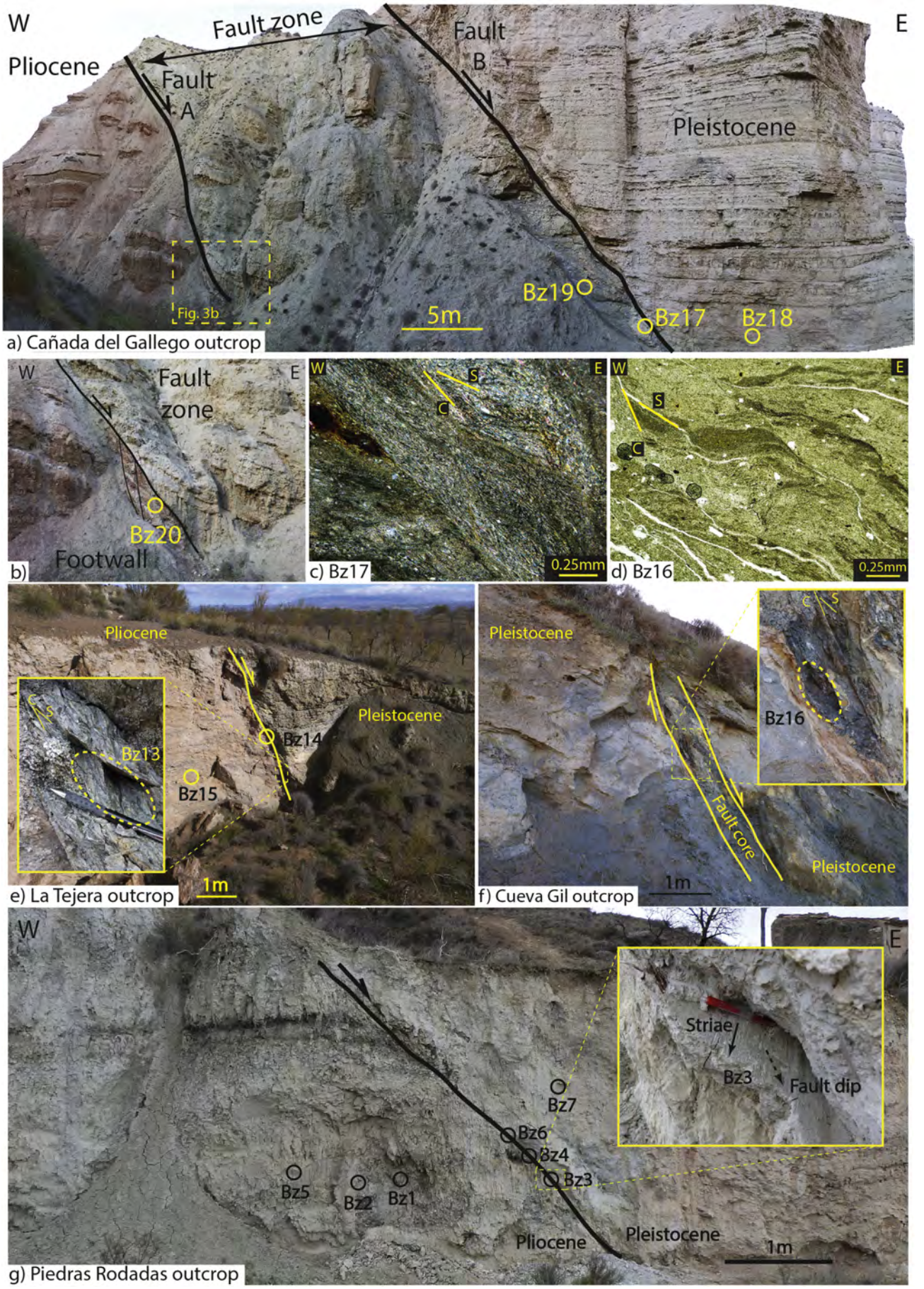
W
Pliocene
Fault zone
Fault A
Fault B
Pleistocene
E
Fig. 3b
5m
Bz19
Bz17
Bz18
a) Cañada del Gallego outcrop
W
Fault zone
E
Bz20
Footwall
b)
W
S
C
E
c) Bz17
0.25mm
W
S
C
E
d) Bz16
0.25mm
Pliocene
C
S
Bz13
Bz15
Bz14
Pleistocene
1m
e) La Tejera outcrop
Pleistocene
C
S
Bz16
Fault core
Pleistocene
1m
f) Cueva Gil outcrop
W
E
Striae
Bz3
Fault dip
Bz7
Bz6
Bz4
Bz3
Bz5
Bz2
Bz1
Pliocene
Pleistocene
1m
g) Piedras Rodadas outcrop

Figure 3

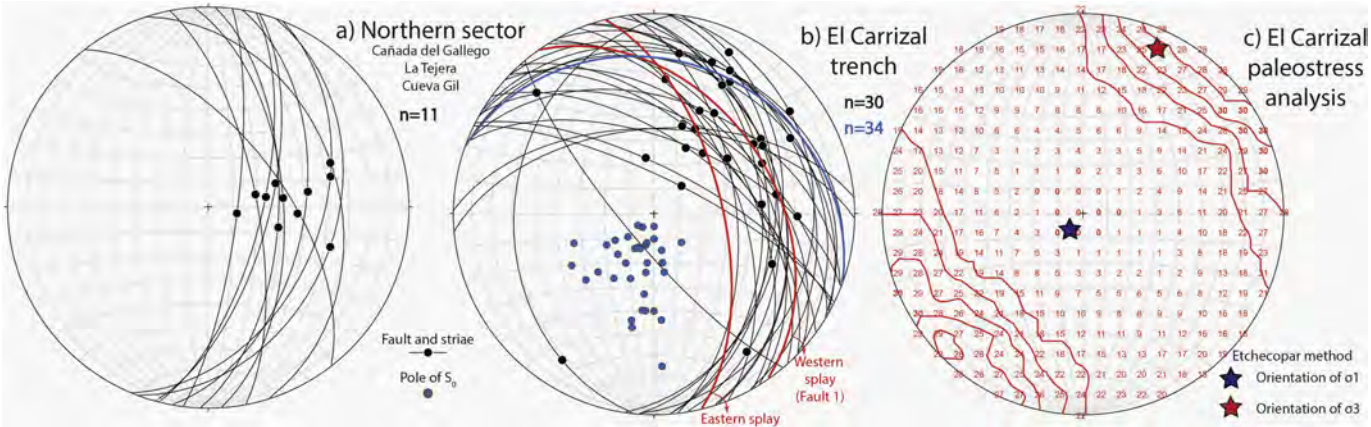
a) Northern sector
Cañada del Gallego
La Tejera
Cueva Gil
n=11
Fault and striae
Pole of S0
b) El Carrizal trench
n=30
n=34
Western splay (Fault 1)
Eastern splay
c) El Carrizal paleostress analysis
Etchecopar method
Orientation of σ1
Orientation of σ3

Figure 4

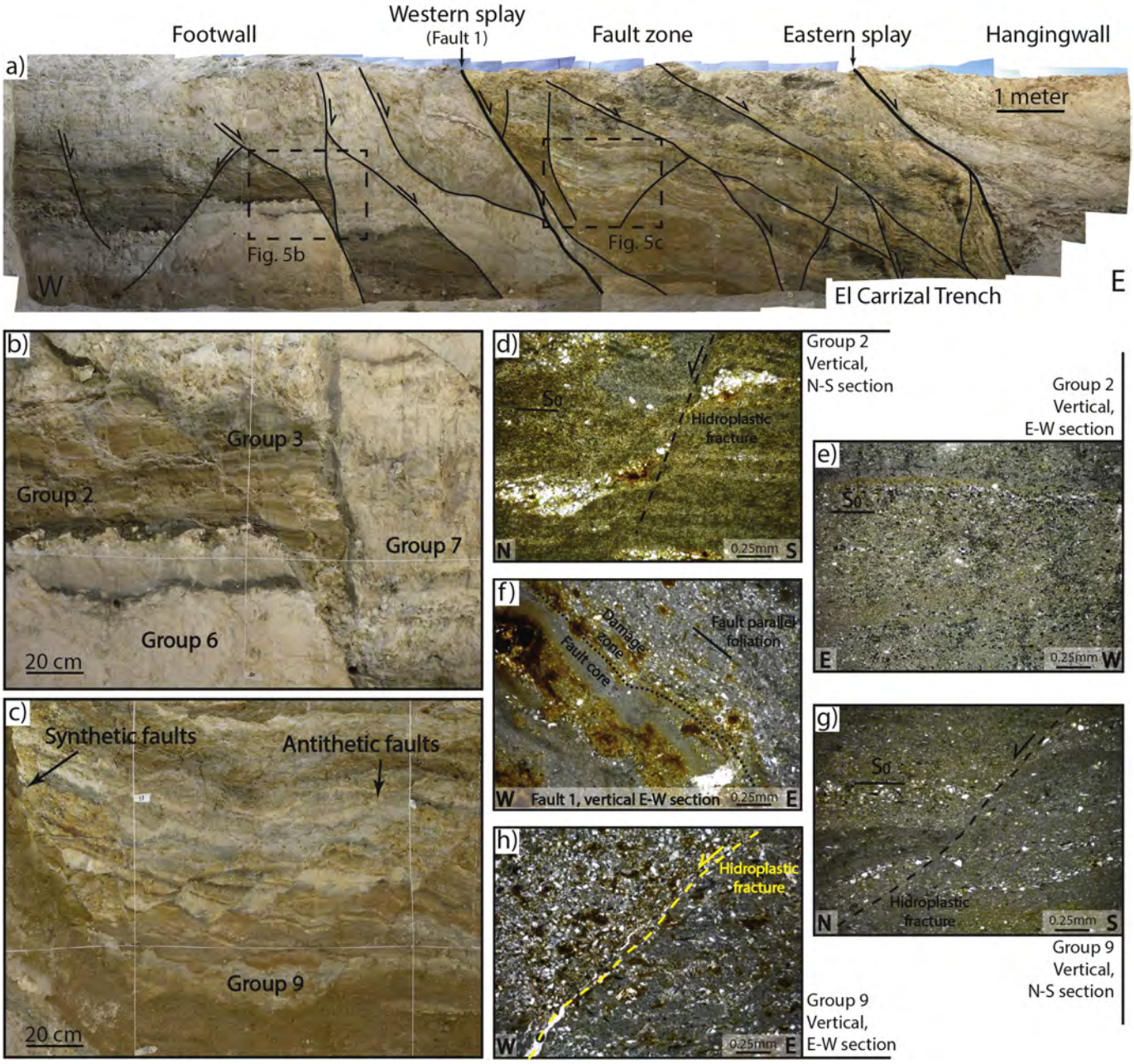
a)
Footwall
Western splay
(Fault 1)
Fault zone
Eastern splay
Hangingwall
1 meter
Fig. 5b
Fig. 5c
W
El Carrizal Trench
E
b)
Group 3
Group 2
Group 7
Group 6
20 cm
c)
Synthetic faults
Antithetic faults
Group 9
20 cm
d)
S0
Hidroplastic fracture
N
0.25mm
S
Group 2
Vertical,
N-S section
Group 2
Vertical,
E-W section
e)
S0
E
0.25mm
W
f)
Damage zone
Fault core
Fault parallel foliation
W
Fault 1, vertical E-W section
0.25mm
E
g)
S0
Hidroplastic fracture
N
0.25mm
S
Group 9
Vertical,
N-S section
h)
Hidroplastic fracture
W
0.25mm
E
Group 9
Vertical,
E-W section

Figure 5

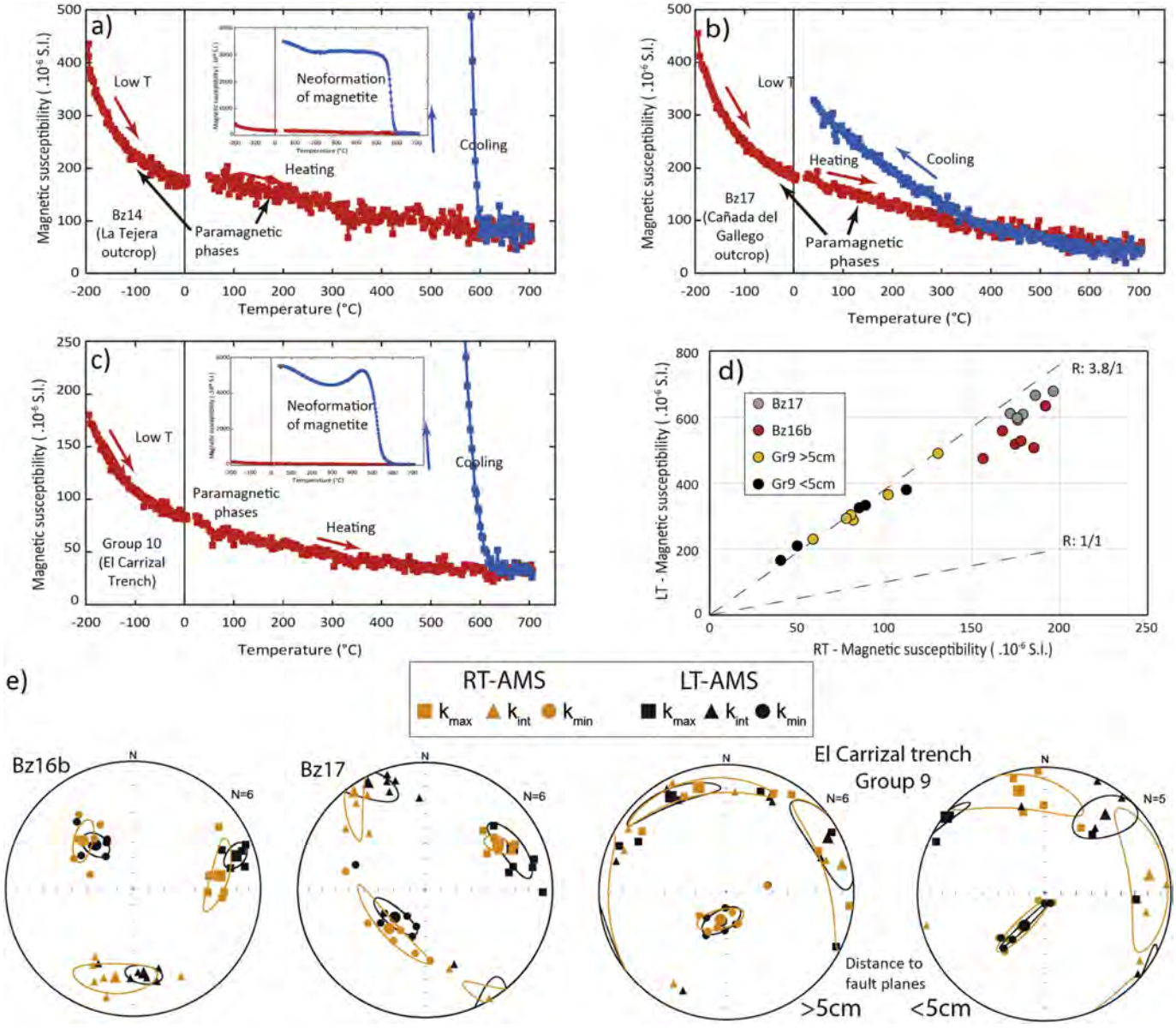
a)
Low T
Neoformation of magnetite
Heating
Cooling
Bz14 (La Tejera outcrop)
Paramagnetic phases
Magnetic susceptibility (.10⁻⁶ S.I.)
Temperature (°C)
b)
Low T
Heating
Cooling
Bz17 (Cañada del Gallego outcrop)
Paramagnetic phases
Magnetic susceptibility (.10⁻⁶ S.I.)
Temperature (°C)
c)
Low T
Neoformation of magnetite
Cooling
Paramagnetic phases
Heating
Group 10 (El Carrizal Trench)
Magnetic susceptibility (.10⁻⁶ S.I.)
Temperature (°C)
d)
R: 3.8/1
R: 1/1
Bz17
Bz16b
Gr9 >5cm
Gr9 <5cm
LT - Magnetic susceptibility (.10⁻⁶ S.I.)
RT - Magnetic susceptibility (.10⁻⁶ S.I.)
e)
RT-AMS
LT-AMS
k_max k_int k_min
Bz16b
N=6
Bz17
N=6
El Carrizal trench
Group 9
N=6
N=5
Distance to fault planes
>5cm
<5cm

Figure 6

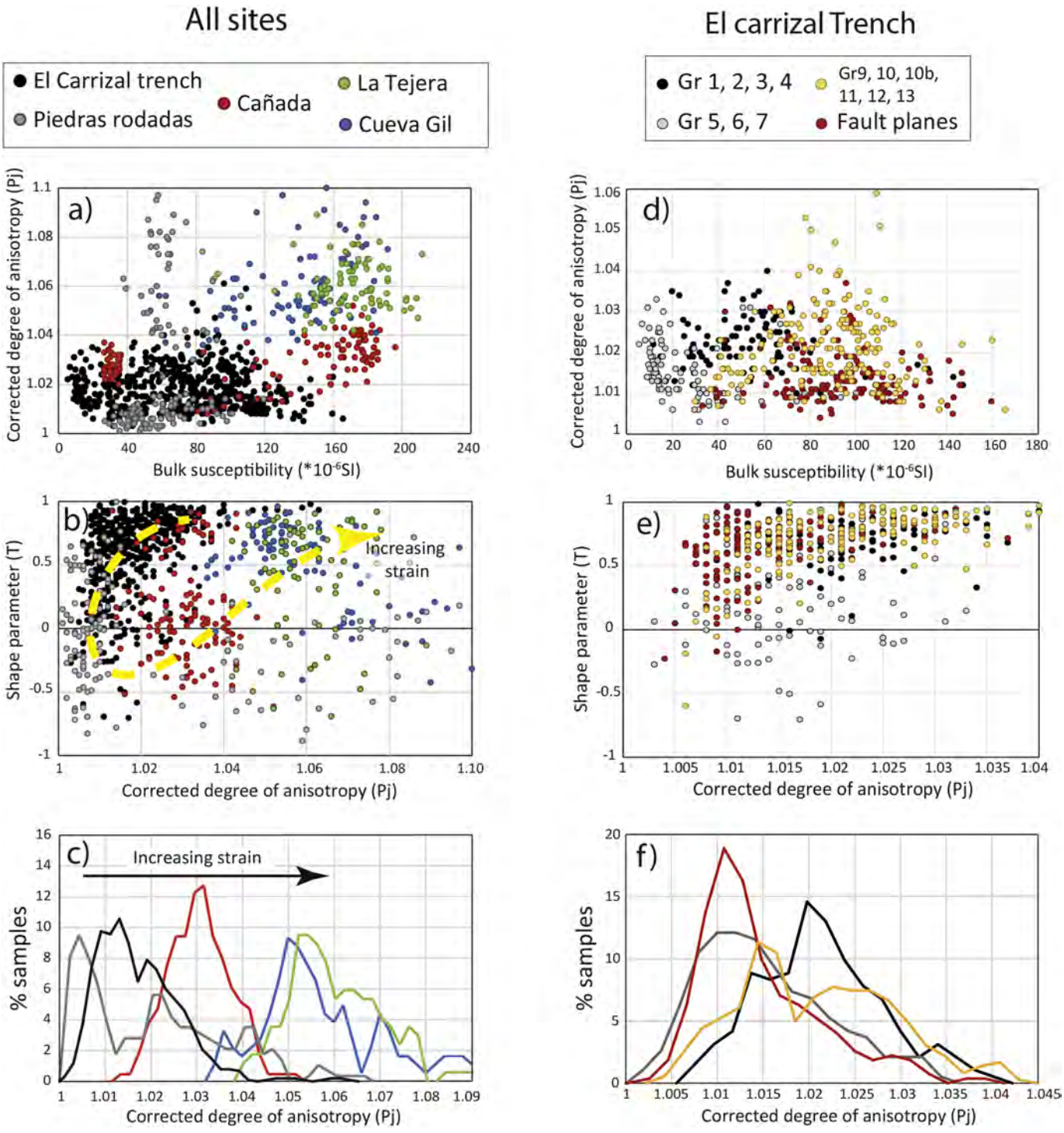
All sites
El Carrizal trench
Piedras rodadas
Cañada
La Tejera
Cueva Gil
a)
Corrected degree of anisotropy (Pj)
Bulk susceptibility (*10-6SI)
b)
Increasing strain
Shape parameter (T)
Corrected degree of anisotropy (Pj)
c)
Increasing strain
% samples
Corrected degree of anisotropy (Pj)
El carrizal Trench
Gr 1, 2, 3, 4
Gr 5, 6, 7
Gr9, 10, 10b, 11, 12, 13
Fault planes
d)
Corrected degree of anisotropy (Pj)
Bulk susceptibility (*10-6SI)
e)
Shape parameter (T)
Corrected degree of anisotropy (Pj)
f)
% samples
Corrected degree of anisotropy (Pj)

Figure 7

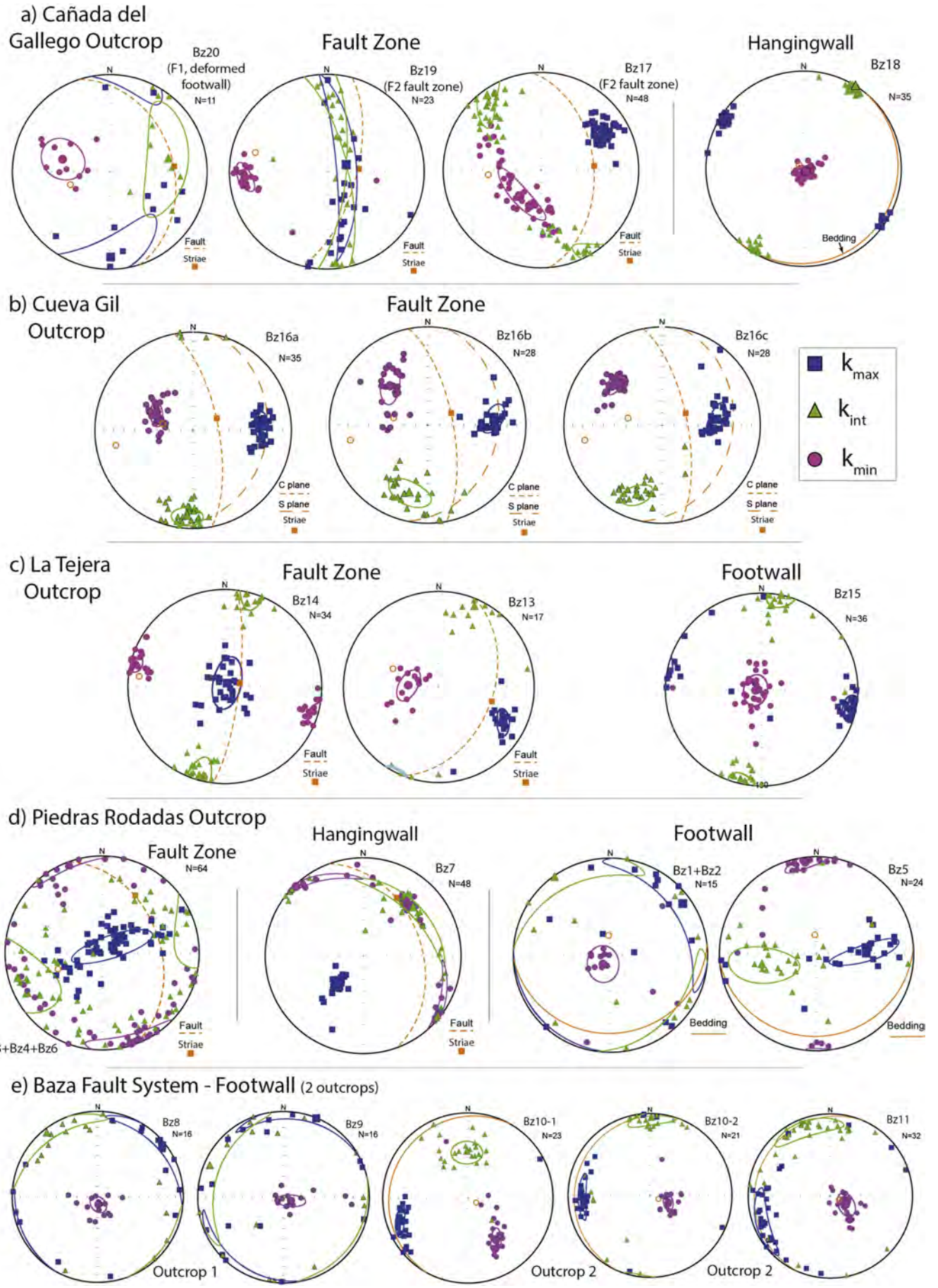
a) Cañada del Gallego Outcrop
Fault Zone
Hangingwall
Bz20 (F1, deformed footwall) N=11
Bz19 (F2 fault zone) N=23
Bz17 (F2 fault zone) N=48
Bz18 N=35
Bedding
Fault
Striae
b) Cueva Gil Outcrop
Fault Zone
Bz16a N=35
Bz16b N=28
Bz16c N=28
C plane
S plane
Striae
k max
k int
k min
c) La Tejera Outcrop
Fault Zone
Footwall
Bz14 N=34
Bz13 N=17
Bz15 N=36
d) Piedras Rodadas Outcrop
Fault Zone N=64
Hangingwall
Footwall
Bz7 N=48
Bz1+Bz2 N=15
Bz5 N=24
Bz3+Bz4+Bz6
e) Baza Fault System - Footwall (2 outcrops)
Bz8 N=16
Bz9 N=16
Bz10-1 N=23
Bz10-2 N=21
Bz11 N=32
Outcrop 1
Outcrop 2
Outcrop 2

Figure 8

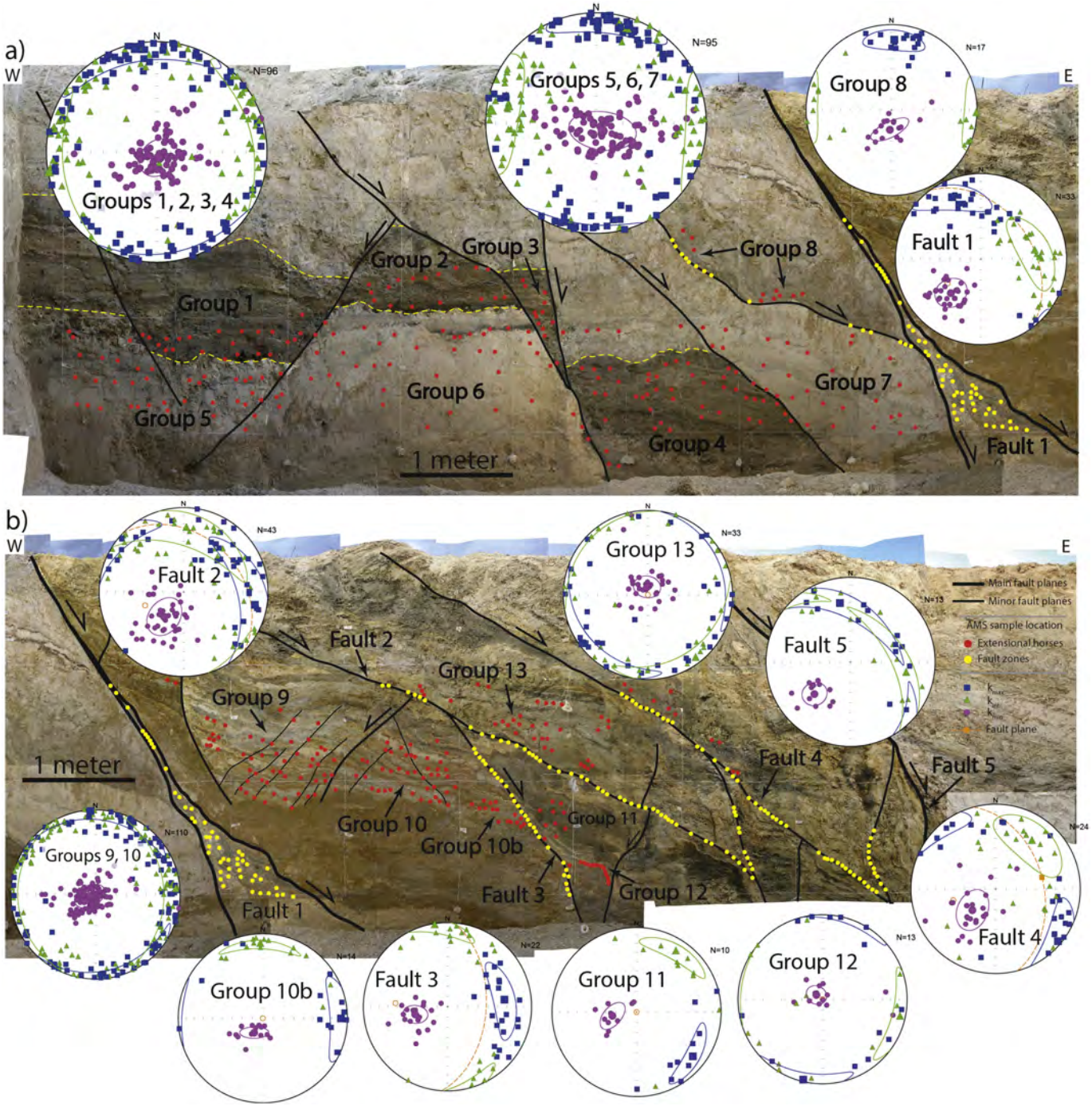
a)
W
E
N=96
Groups 1, 2, 3, 4
N=95
Groups 5, 6, 7
N=17
Group 8
N=33
Fault 1
Group 1
Group 2
Group 3
Group 5
Group 6
Group 4
Group 7
Group 8
Fault 1
1 meter
b)
W
E
N=43
Fault 2
N=33
Group 13
N=13
Fault 5
Main fault planes
Minor fault planes
AMS sample location
Extensional horses
Fault zones
Fault plane
Fault 2
Group 13
Group 9
1 meter
Fault 4
Fault 5
Group 10
Group 10b
Group 11
Fault 3
Group 12
Fault 1
N=110
Groups 9, 10
N=24
Fault 4
N=14
Group 10b
N=22
Fault 3
N=10
Group 11
N=13
Group 12

Figure 9

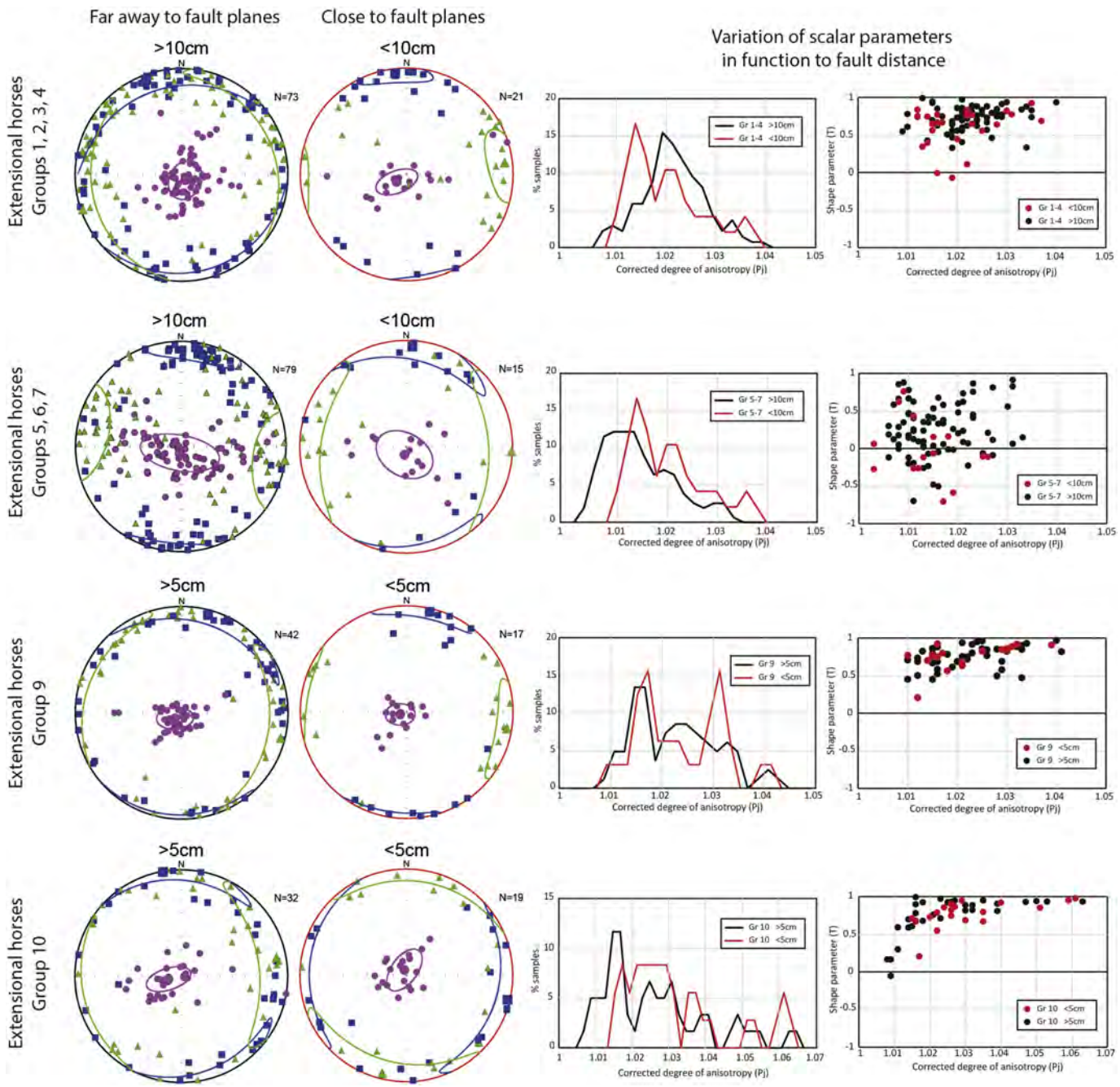
Far away to fault planes
Close to fault planes
Variation of scalar parameters in function to fault distance
Extensional horses Groups 1, 2, 3, 4
>10cm
<10cm
N=73
N=21
Gr 1-4 >10cm
Gr 1-4 <10cm
% samples
Shape parameter (T)
Corrected degree of anisotropy (Pj)
Extensional horses Groups 5, 6, 7
N=79
N=15
Gr 5-7 >10cm
Gr 5-7 <10cm
Extensional horses Group 9
>5cm
<5cm
N=42
N=17
Gr 9 >5cm
Gr 9 <5cm
Extensional horses Group 10
N=32
N=19
Gr 10 >5cm
Gr 10 <5cm

Figure 10

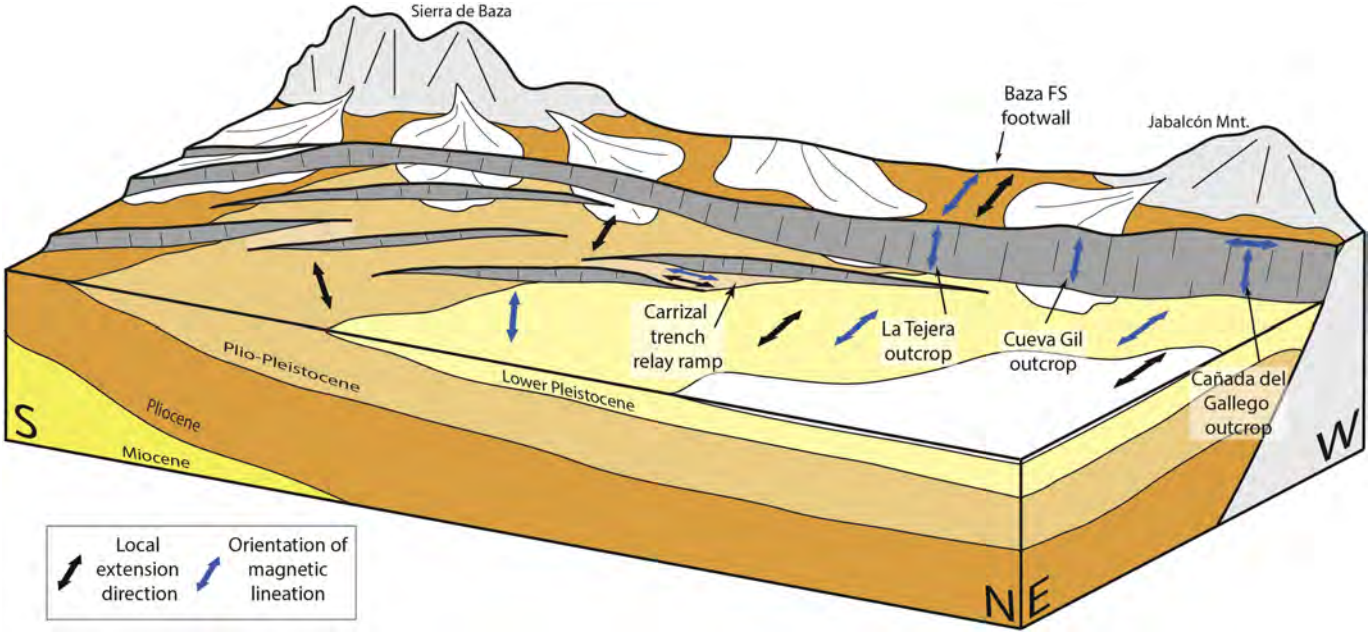
Sierra de Baza
Baza FS footwall
Jabalcón Mnt.
Carrizal trench relay ramp
La Tejera outcrop
Cueva Gil outcrop
Cañada del Gallego outcrop
Plio-Pleistocene
Lower Pleistocene
Pliocene
Miocene
S
W
N
E
Local extension direction
Orientation of magnetic lineation

Figure 11

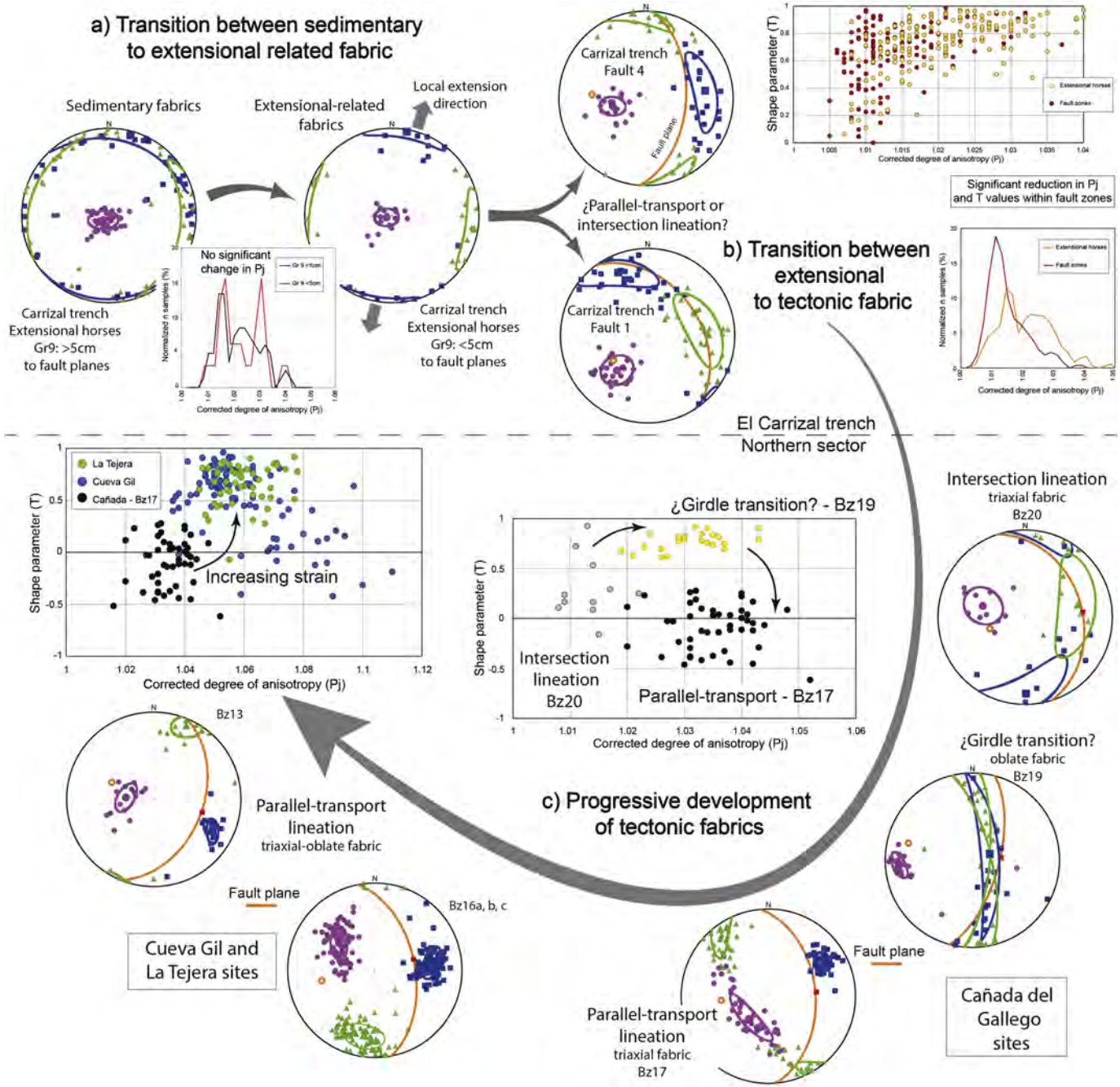
a) Transition between sedimentary to extensional related fabric
Sedimentary fabrics
Extensional-related fabrics
Local extension direction
Carrizal trench
Extensional horses
Gr9: >5cm
to fault planes
No significant change in Pj
Carrizal trench
Extensional horses
Gr9: <5cm
to fault planes
Carrizal trench
Fault 4
Fault plane
¿Parallel-transport or intersection lineation?
Carrizal trench
Fault 1
Shape parameter (T)
Corrected degree of anisotropy (Pj)
Extensional horses
Fault zones
Significant reduction in Pj and T values within fault zones
b) Transition between extensional to tectonic fabric
Normalized n samples (%)
El Carrizal trench
Northern sector
La Tejera
Cueva Gil
Cañada - Bz17
Increasing strain
¿Girdle transition? - Bz19
Intersection lineation
Bz20
Parallel-transport - Bz17
Intersection lineation
triaxial fabric
Bz20
Bz13
Parallel-transport lineation
triaxial-oblate fabric
c) Progressive development of tectonic fabrics
¿Girdle transition?
oblate fabric
Bz19
Fault plane
Bz16a, b, c
Cueva Gil and La Tejera sites
Parallel-transport lineation
triaxial fabric
Bz17
Fault plane
Cañada del Gallego sites

Figure 12